iScience

CellPress
OPEN ACCESS

Article

Diffusion of small molecule drugs is affected by surface interactions and crowder proteins

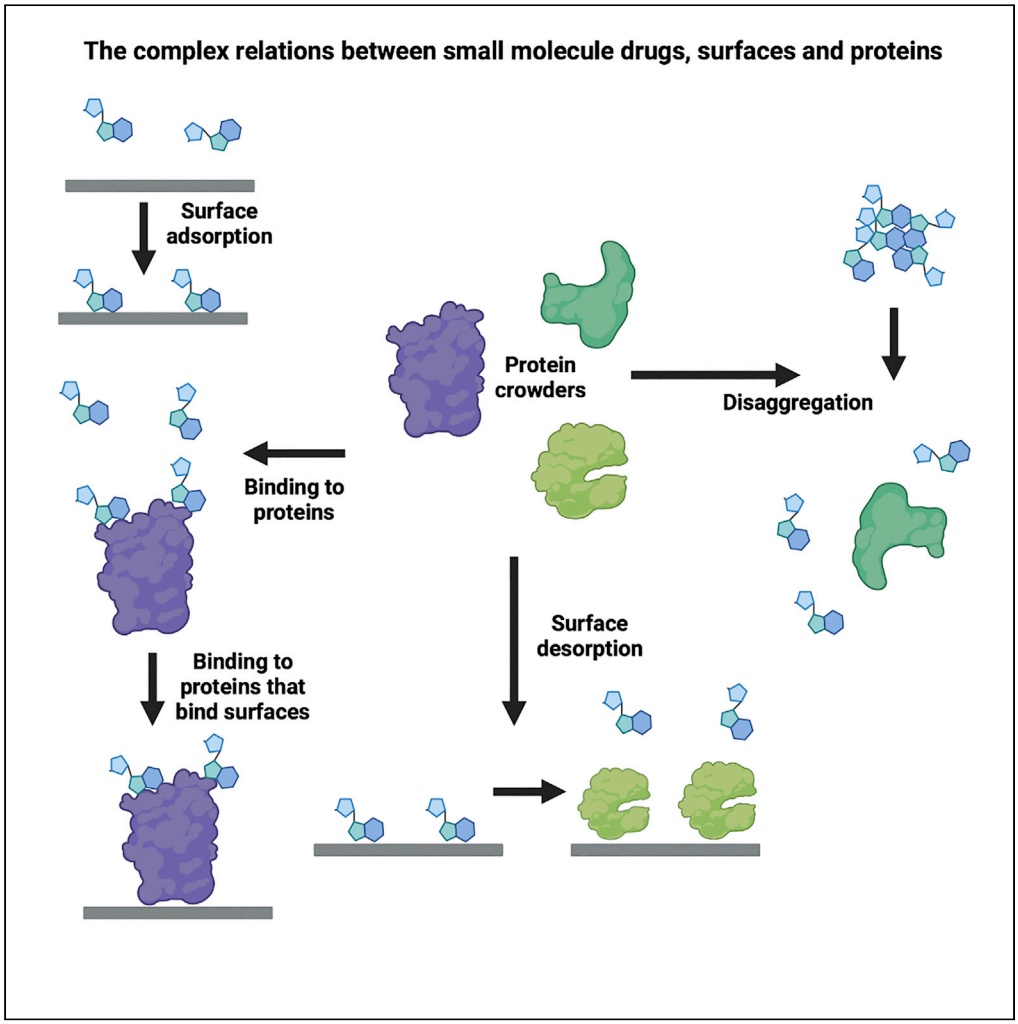

Debabrata Dey, Ariane Nunes-Alves, Rebecca C. Wade, Gideon Schreiber

rebecca.wade@h-its.org (R.C.W.)
gideon.schreiber@weizmann.ac.il (G.S.)

Highlights

Diffusion of small molecule drugs is strongly affected by the surroundings

Aggregation, binding to proteins and surface adsorption dictate drug diffusion

Experimental methods and simulations revealed the mechanisms affecting diffusion

Proteins may increase drug diffusion by shielding from surfaces and aggregation

Dey et al., iScience 25, 105088
October 21, 2022
https://doi.org/10.1016/j.isci.2022.105088

iScience

CellPress
OPEN ACCESS

Article

Diffusion of small molecule drugs is affected by surface interactions and crowder proteins

Debabrata Dey,[1,6] Ariane Nunes-Alves,[2,3,5,6] Rebecca C. Wade,[2,3,4,*] and Gideon Schreiber[1,7,*]

SUMMARY

Crowded environments are known to affect the diffusion of macromolecules, but their effects on the diffusion of small molecules are largely uncharacterized. We investigate how three protein crowders, bovine serum albumin (BSA), hen egg-white lysozyme, and myoglobin, influence the diffusion rates and interactions of four small molecules: fluorescein, and three drugs, doxorubicin, glycogen synthase kinase-3 inhibitor SB216763, and quinacrine. Using Line-FRAP measurements, Brownian dynamics simulations, and molecular docking, we find that the diffusion rates of the small molecules are highly affected by self-aggregation, interactions with the proteins, and surface adsorption. The diffusion of fluorescein is decreased because of its interactions with the protein crowders and their surface adsorption. Protein crowders increase the diffusion rates of doxorubicin and SB216763 by reducing surface interactions and self-aggregation, respectively. Quinacrine diffusion was not affected by protein crowders. The mechanistic insights gained here may assist in optimization of compounds for higher mobility in complex macromolecular environments.

INTRODUCTION

Most drugs have a molecular weight <1 kDa and an octanol/water partition (logP) of 1–6 (Lipinski et al., 1997). For a drug to be orally absorbed, it must be hydrophobic to partition into a lipid bilayer, but not to such an extent that it will result in permanent absorbance into the bilayer (Lipinski et al., 1997). This property results in drugs being able to self-associate and bind to hydrophobic cellular components through soft interactions (Schreier et al., 2000), which in turn decreases their active concentration and affects their diffusion. In addition to self-aggregation in polar aqueous or buffer-like solvents, small molecule drugs tend to interact with or adsorb to glass or plastic surfaces, further complicating diffusion measurements (Curry et al., 2015). Overlooking these factors may lead to spurious observations that can negatively impact studies of small molecule drugs (Feng et al., 2007; Owen et al., 2012). Moreover, although biophysical characterization of such drugs is carried out *in vitro*, they are required to be active in a complex, crowded environment, containing membranes and macromolecules at concentrations of up to 300 mg/mL (Zimmerman and Trach, 1991).

For small molecules to reach their target within a crowded milieu, they have to freely diffuse and avoid off-target interactions (Ribeiro et al., 2017). Passive diffusion is considered to be a primary mechanism of intracellular drug transport (Di et al., 2012). However, more recently carrier-mediated transport (Dobson and Kell, 2008; Di et al., 2012) or a combination of the two were also identified (Sugano et al., 2010). The study of the diffusion of small organic molecules inside complex environments is therefore highly relevant for drug design (Ribeiro et al., 2017; Miyamoto and Shimono, 2020), as well as for soft matter and biochemical studies more generally (Kekenes-Huskey et al., 2015; Miguel Rubi, 2019). The challenge is that most small molecules are not fluorescent in the visible spectrum (Feig et al., 2018), making it almost impossible to follow them by optical methods (White and Errington, 2005). Conversely, proteins can usually be fluorescently labeled without significant perturbation of their diffusion rate and function, making it relatively easy to study their diffusion (Zhang et al., 2018).

Here, we investigated the diffusion of three fluorescent organic small molecule therapeutic drugs and one diagnostic marker in solutions containing proteins as crowders. Doxorubicin (DOX) is widely used as an anti-cancer agent (Carvalho et al., 2009); quinacrine dihydrochloride has been used for antimalarial and antiprotozoal therapy (Ehsanian et al., 2011); glycogen synthase kinase-3 (GSK3) inhibitor SB216763 is a

[1]Department of Biomolecular Sciences, Weizmann Institute of Science, Israel

[2]Molecular and Cellular Modeling Group, Heidelberg Institute for Theoretical Studies, Schloss-Wolfsbrunnenweg 35, 69118 Heidelberg, Germany

[3]Center for Molecular Biology (ZMBH), DKFZ-ZMBH Alliance, Heidelberg University, Im Neuenheimer Feld 282, 69120 Heidelberg, Germany

[4]Interdisciplinary Center for Scientific Computing (IWR), Heidelberg University, Im Neuenheimer Feld 205, Heidelberg, Germany

[5]Present address: Institute of Chemistry, Technische Universität Berlin, 10623 Berlin, Germany

[6]These authors contributed equally

[7]Lead contact

*Correspondence: rebecca.wade@h-its.org (R.C.W.), gideon.schreiber@weizmann.ac.il (G.S.)

https://doi.org/10.1016/j.isci.2022.105088

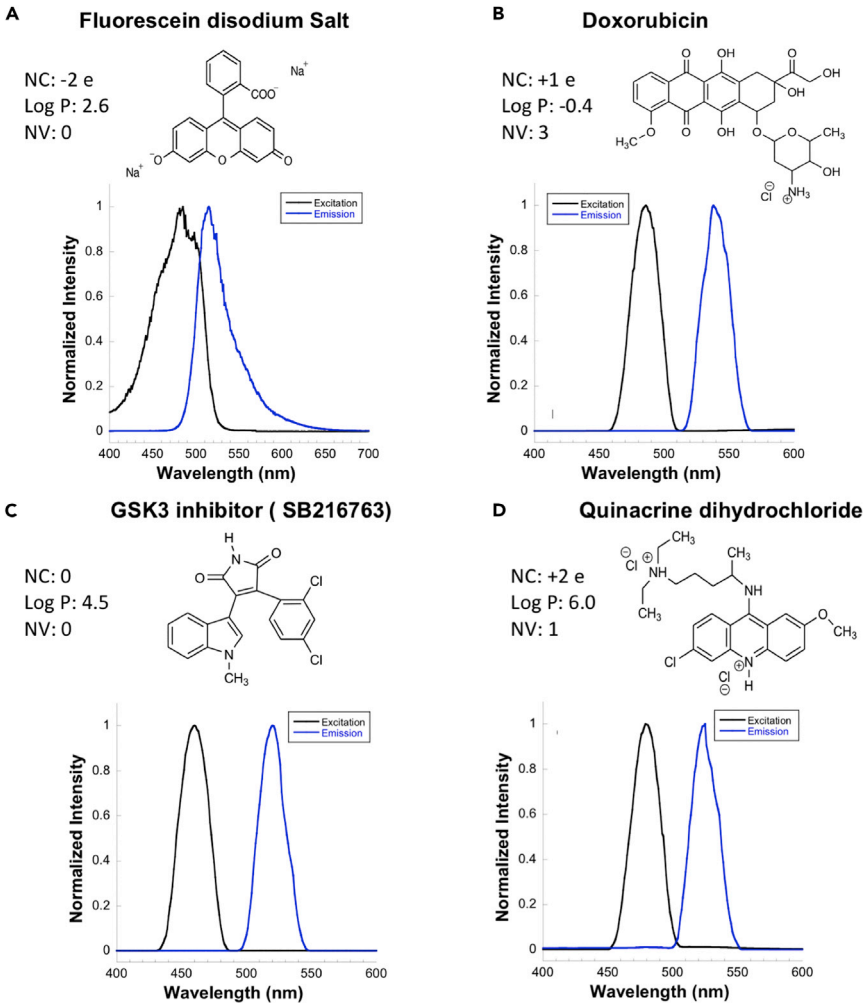

Figure 1. Chemical structures, physicochemical properties and comparative excitation and emission spectra with relative strengths

(A) Fluorescein disodium salt, (B) doxorubicin, (C) GSK3 SB216763 inhibitor, and (D) quinacrine dihydrochloride. NC: net charge at pH 7.2 (computed using Epik (Shelley et al., 2007)). Log P: log of the octanol-water partition coefficient (computed using QikProp (Schrödinger, LLC, New York, 2021)). NV: number of violations to Lipinski's rule of five for drug likeness (computed using QikProp (Schrödinger, LLC, New York, 2021)).

potent selective and ATP-competitive inhibitor of glycogen synthase kinase-3 and significantly prevents lung inflammation and fibrosis in mouse models (Coghlan et al., 2000). DOX and quinacrine behave as weak bases at physiological pH (Zhitomirsky and Assaraf, 2015). Unlike these three therapeutic drugs, fluorescein in its salt form, which is widely used as a biological marker in angiographic assays, is a negatively charged molecule at physiological pH (O'goshi and Serup, 2006). These four molecules were chosen for study as they form a structurally and chemically diverse set of compounds that fluoresce in the visible spectrum, a prerequisite for Line FRAP studies (Figure 1). The diffusion and aggregation of these low molecular weight (MW) molecules were evaluated in buffer, and with BSA, hen egg-white lysozyme (HEWL), or myoglobin as molecular crowders (Miklos et al., 2011; Feig and Sugita, 2012). Self-aggregation and binding to these proteins can potentially mimic their behaviors in body fluids or inside the cell (Seidler et al., 2003). Diffusion rate measurements provide a good means of estimating these protein-ligand associations or the aggregation state of the compounds in diverse environments which affect the mobility of the compounds.

A wide range of computational and experimental techniques have been developed to compute and measure diffusion rates, as well as to study molecular association. On the computational side, Brownian

dynamics (BD) (Huber and McCammon, 2019) and molecular dynamics (MD) simulations are widely used (Feig and Sugita, 2012; Feig et al., 2018; Bullerjahn et al., 2020; Kasahara et al., 2021). In both methods, the system can be considered in atomic detail, but in BD simulations, the molecules are generally treated as rigid bodies and an implicit solvation model is used. These simplifications allow BD simulations to routinely achieve tens of microseconds of simulation time with systems containing hundreds of solute molecules. BD simulations have been previously employed to compute diffusional properties of proteins, revealing, for example, molecular details about the reduction in diffusion rates of BSA, myoglobin, hemoglobin and γ-globulin under crowding conditions (Mereghetti and Wade, 2012; Balbo et al., 2013) or the adsorption of HEWL to an inorganic surface (Romanowska et al., 2015; Reinhardt et al., 2021).

Among the experimental techniques, fluorescence recovery after photobleaching (FRAP) (Lorén et al., 2015), fluorescence correlation microscopy (FCS) (Dauty and Verkman, 2004), and single-particle tracking (SPT) (Manley et al., 2008) are the most popular. Each method has its benefits and limitations (Deschout et al., 2014). FCS is considered the gold standard for this purpose; however, its application can be challenging. First, it requires high quantum yield (which is rare for drugs), and second, it can be performed only at very low concentrations, which may be much lower than found *in vivo*. Therefore, FRAP is the technique most widely used by experimental biologists (Deschout et al., 2014). It is fast, non-invasive, highly specific, and relatively easy to perform (Deschout et al., 2014). Moreover, FRAP can be used for molecules with poor quantum yields and at high, biologically relevant concentrations (Lorén et al., 2015).

We previously developed the fluorescence recovery after photobleaching in line mode (Line-FRAP) method to monitor the diffusion rates of proteins in various environments (Dey et al., 2021). The main advantage of Line-FRAP over conventional FRAP is the much faster data acquisition rate, which allows measurements for fast diffusing molecules. The apparent diffusion coefficients derived from FRAP measurements are $D_{confocal}$ (Dey et al., 2021), which are calculated according to Equation 1:

$$D_{confocal} = \frac{r_e^2 + r_n^2}{8\tau_{1/2}} \quad \text{(Equation 1)}$$

where $\tau_{1/2}$ is the half-time of recovery and r_e and r_n are the effective and nominal bleach radii. Line-FRAP $D_{confocal}$ values were shown to be in line with FCS diffusion rates for proteins (Dey et al., 2021). However, for small molecules, they provide only relative 3D diffusion coefficients (Hoffmann et al., 2009). An alternative way to present FRAP results is by reporting only $\tau_{1/2}$ values. However, as seen from Equation (1), this completely ignores the contribution from the bleach radius (which is squared) (Axelrod et al., 1976; Soumpasis, 1983). In particular, r_e varies, depending on the type of molecule and the diffusion condition, making its measurement critical to obtain reliable estimates of diffusion rates (Dey et al., 2021).

In this study, we determined $D_{confocal}$ values by Line-FRAP for the four low molecular weight compounds using the three different proteins as crowders. The derived diffusion coefficients are found to depend on the self-aggregation properties of the small molecules, their binding to proteins and surfaces, and the buffer solution conditions. The protein crowders affect the solubility and diffusion rates of the compounds in a manner that is dependent on the properties of the different protein crowders used. Complementary steady-state fluorescence quenching and size exclusion chromatography experiments provide affinity data that reveal differences in the association between the compounds and the protein crowders. Furthermore, BD simulations and molecular docking for the systems studied experimentally shed light on the intermolecular interactions and molecular mechanisms responsible for the differences in the diffusion coefficients measured for the different small molecule and protein crowder combinations.

RESULTS

We used high-content screening of over 1000 drugs and the database fluorophores.org to search for drugs that are fluorescent in visible light, allowing us to follow their diffusion using FRAP. Of those identified, we chose fluorescein, DOX, SB216763, and quinacrine for this study, as they have moderate to good quantum yields.

Fluorescein disodium salt

Fluorescein is a negatively charged organic small molecule (MW = 376.3 Da, Figure 1A). We first measured the diffusion rates of fluorescein in different solvents with and without protein crowders. The values of $D_{confocal}$ in DMSO and PBS, with and without Tween20, are given in Figures 2A. Figure 2B shows

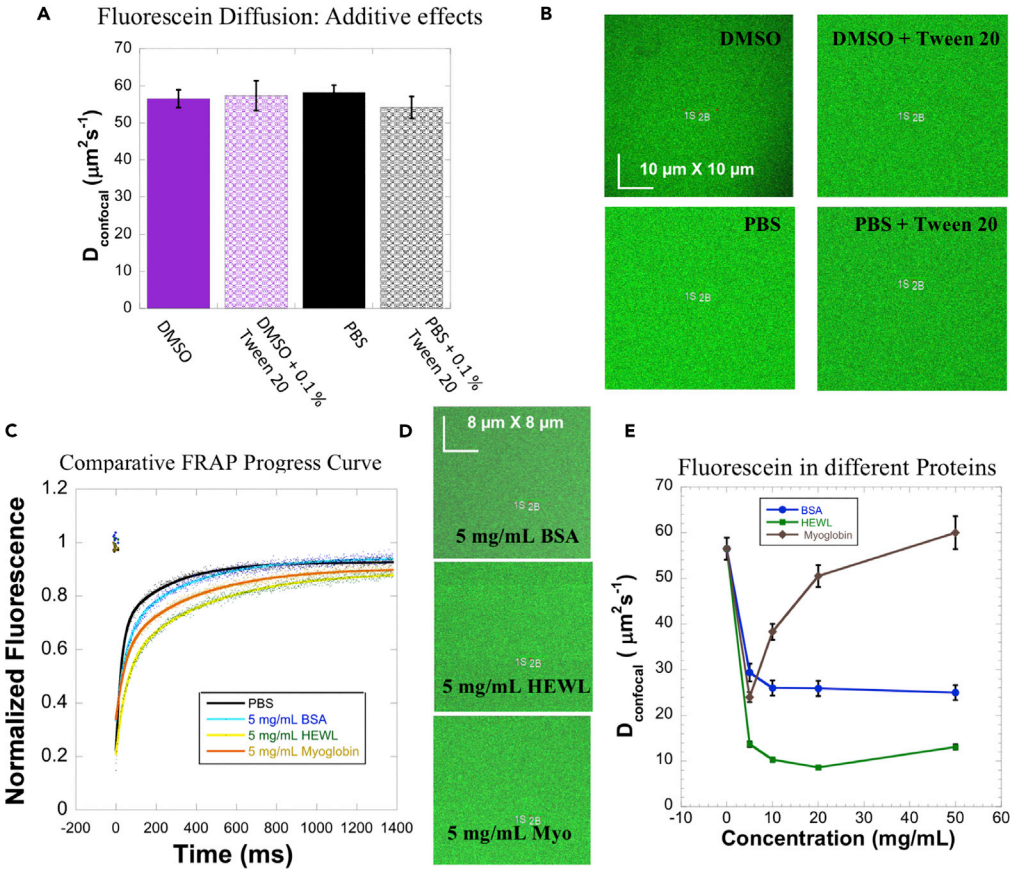

Figure 2. Fluorescein in buffer and in the presence of protein crowders

(A and B) Diffusion coefficients (A) and images from confocal microscopy (B) of fluorescein in DMSO or PBS with or without Tween 20.

(C and D) Comparative averaged FRAP profiles (N= 30; R= 0.99 for each of the fits) (C) and images from confocal microscopy (D) of fluorescein in the presence of 5 mg/mL BSA, HEWL or myoglobin.

(E) Diffusion coefficients of fluorescein from measurements at increasing concentrations of the three protein crowders. Error bars represent SE calculated from fitting the FRAP progression curves, which are averaged over at least 30 independent measurements (see STAR methods).

micrograph images of fluorescein in corresponding solutions. A $D_{confocal}$ value of ~56 $\mu m^2 s^{-1}$ was determined in all these cases, and there was no evidence for aggregation of fluorescein. Next, we measured fluorescein's diffusion in the presence of increasing concentrations of BSA, HEWL, and myoglobin (Figures 2C–2E). We were surprised to see that, even at low concentrations of protein (5–20 mg/mL), the presence of BSA, HEWL and myoglobin significantly slowed down the diffusion of fluorescein (Figure 2E). Because the fraction of excluded volume from the presence of protein crowders at these concentrations is low, we suspected that quinary or weak interactions between fluorescein and the protein crowders are the main drivers of the reduction in the diffusion rates of fluorescein, in line with previous publications (von Bülow et al., 2019). HEWL had the biggest effect on diffusion, followed by BSA and myoglobin. Of interest, for myoglobin, increasing protein concentrations above 5 mg/mL resulted in an increase in diffusion rates, which returned to their level without crowder at 50 mg/mL (Figure 2E). As in the absence of protein crowders (Figure 2B), micrographs in the presence of protein crowders did not show aggregation (Figure 2D) and FRAP fully recovered after bleach under all conditions measured (Figure 2C).

Next, we compared the diffusion of fluorescein and labeled BSA to test if the reduction in the diffusion rates of fluorescein in the presence of BSA could be explained solely by interactions with BSA in solution (Figure 3A). Unexpectedly, we observed that the diffusion coefficients of labeled BSA were higher than those of fluorescein in the presence of BSA for all concentrations of BSA tested. This observation implies that the

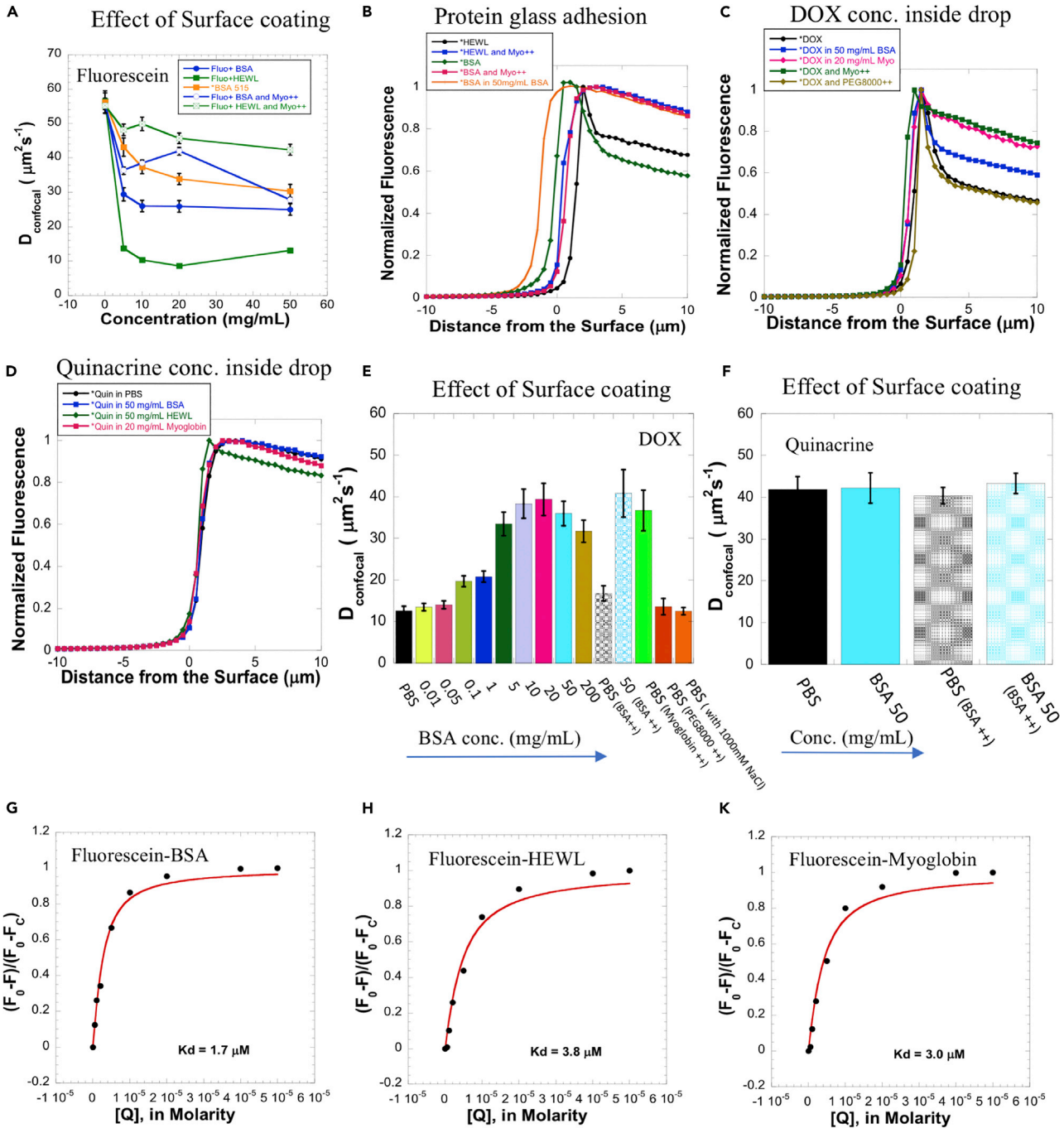

Figure 3. Adsorption of drugs and protein crowders to a glass surface

(A) Effect of pre-surface coating of glass plates by myoglobin (indicated by Myo++) on the diffusion coefficient of fluorescein with BSA or with HEWL. Diffusion of a labeled protein is defined by * before the protein (for example, *BSA).

(B–D) Determination of drop homogeneity of (B) labeled proteins (protein-glass adhesion) in different crowding environments and in buffer solutions with or without pre-surface coating. (C) Determination of drop homogeneity for solutions containing doxorubicin, or (D) quinacrine.

(E and F) Effect on diffusion coefficients by increasing concentrations of BSA or by surface pre-coating of glass plates for (E) doxorubicin, or (F) quinacrine. The asterik (*) symbol denotes labeling of the protein, and ++ symbol denotes glass pre-coating.

(G–K) Determination of binding affinities of fluorescein to the three protein crowders by fluorescence quenching in PBS buffer. $(F_0\text{-}F)/(F_0\text{-}F_c)$ versus [Q] plots of the data and fits (R = 0.99), where [Q] is the titrating drug concentration in molarity, are shown. Micromolar binding affinities were determined for fluorescein to all three protein crowders.

Error bars represent SE calculated from fitting the FRAP progression curves, which are averaged over at least 30 independent measurements (see STAR methods).

reduced diffusion coefficient of fluorescein in the presence of BSA cannot be solely explained by binding of fluorescein to freely diffusing BSA.

However, these experiments were performed on liquid drops on a glass surface, and if BSA was adsorbed to the glass surface, this could lead to a reduction in the diffusion of BSA-bound fluorescein molecules. To directly assess this possibility, a drop containing labeled BSA or labeled HEWL was applied to the glass, and the fluorescence along the z axis perpendicular to the plane of the glass surface was measured (Figure 3B). Clearly, both proteins attach to the surface, as seen by the higher fluorescence close to the surface. Next, we pre-coated the glass slides either with unlabeled BSA or with myoglobin, washed the glass, and then applied labeled BSA or HEWL (Figure 3B). Now, the fluorescence profile indicated that the labeled protein became rather homogeneously distributed along the z axis above the surface, indicating lack of adsorption of labeled protein to the glass. Repeating the FRAP measurements of fluorescein in the presence of either HEWL or BSA, but this time after pre-coating the glass with myoglobin (Figure 3A), resulted in much higher diffusion coefficients for fluorescein. In the presence of increasing concentrations of BSA, the $D_{confocal}$ values for fluorescein were similar to those measured for labeled BSA. Furthermore, after coating the surface with myoglobin, the presence of HEWL had only a small effect on the diffusion coefficient of fluorescein, in contrast to the large reduction in $D_{confocal}$ without pre-coating. As fluorescein alone in PBS or in the presence of protein crowders does not attach to the glass surface (Figure S1A), the experimental data suggest that fluorescein's reduced diffusion is because of its attachment to the proteins bound to the glass surface. This conclusion is supported by dynamic light scattering (DLS) experiments to measure the hydrodynamic size of BSA alone and in the presence of fluorescein at different protein and fluorescein concentrations (Figure S2). The hydrodynamic size (in nm) of BSA did not change on addition of fluorescein to different concentrations of BSA or even when the added fluorescein concentration was 10 times that used in the FRAP measurements. This shows that fluorescein does not affect the oligomerization state of BSA and that its interaction with freely diffusing BSA would be expected to give a diffusion coefficient corresponding to that of BSA, which is higher than observed in the experiments.

To quantify the protein-small molecule binding affinities, steady-state fluorescence quenching experiments were carried out. The association of the small molecules with the proteins causes a change in the environment around buried tryptophan residues (which are largely responsible for the intrinsic fluorescence properties of proteins), which results in the quenching of fluorescent signals from the protein (Agudelo et al., 2012). For example, BSA contains two tryptophan residues, Trp-134 and Trp-212, located in the first and second domains of hydrophobic protein regions (Agudelo et al., 2012). The decrease of fluorescence intensity for BSA was monitored at 344 nm wavelength for the drug-protein pairs. Figures S3A–S3C show representative fluorescence quench spectra for fluorescein with BSA, HEWL, and myoglobin. We assume that the observed changes in the fluorescence are the result of the interaction between the small molecule and the protein. Therefore, corresponding plots of $(F_0\text{-}F)/(F_0\text{-}F_c)$ versus fluorescein concentration [Q] in molarity (Figures 3G–3K) were used to determine the affinity between them, using Equation 2 (see STAR Methods). BSA, HEWL, and myoglobin were found to bind fluorescein with affinities of 1.7 $\pm$ 0.2 μM, 3.8 $\pm$ 0.6 μM and 3.0 $\pm$ 0.5 μM, respectively (Figures 3G–3K and Table S1).

To further investigate the factors influencing the diffusion of fluorescein, BD simulations were performed for fluorescein and the same concentrations of protein crowders as present in the FRAP experiments. The results show that the effects of the crowders modeled in these simulations (excluded volume, electrostatic and hydrophobic interactions between rigid solutes) result in modest reductions of up to 15% in the computed translational diffusion coefficients of the small molecules at crowder concentrations up to 50 mg/mL (Figure S4). This is roughly in line with the reduction in $D_{confocal}$ observed for fluorescein and HEWL and BSA crowders after pre-coating the glass slide with myoglobin. The BD simulations also revealed differences in the interactions of fluorescein with the three protein crowders which were examined by computing the number of intermolecular contact interactions. Contacts were defined as present if non-hydrogen atoms (at least one in a protein crowder and at least one in a small molecule) were within 4.5 Å of each other. This distance was chosen to capture electrostatic and van der Waals interactions between protein crowders and fluorescein. The number of protein-fluorescein contact interactions (Figure 4A) and the peak of the radial distribution function (RDF) for protein-small molecule distances (Figure 4B) are higher in the presence of HEWL, showing that the interactions of fluorescein are stronger with this protein crowder. The stronger interactions between fluorescein and HEWL are consistent with the experimentally observed stronger reduction in the diffusion coefficient of fluorescein in the presence of HEWL than in the presence

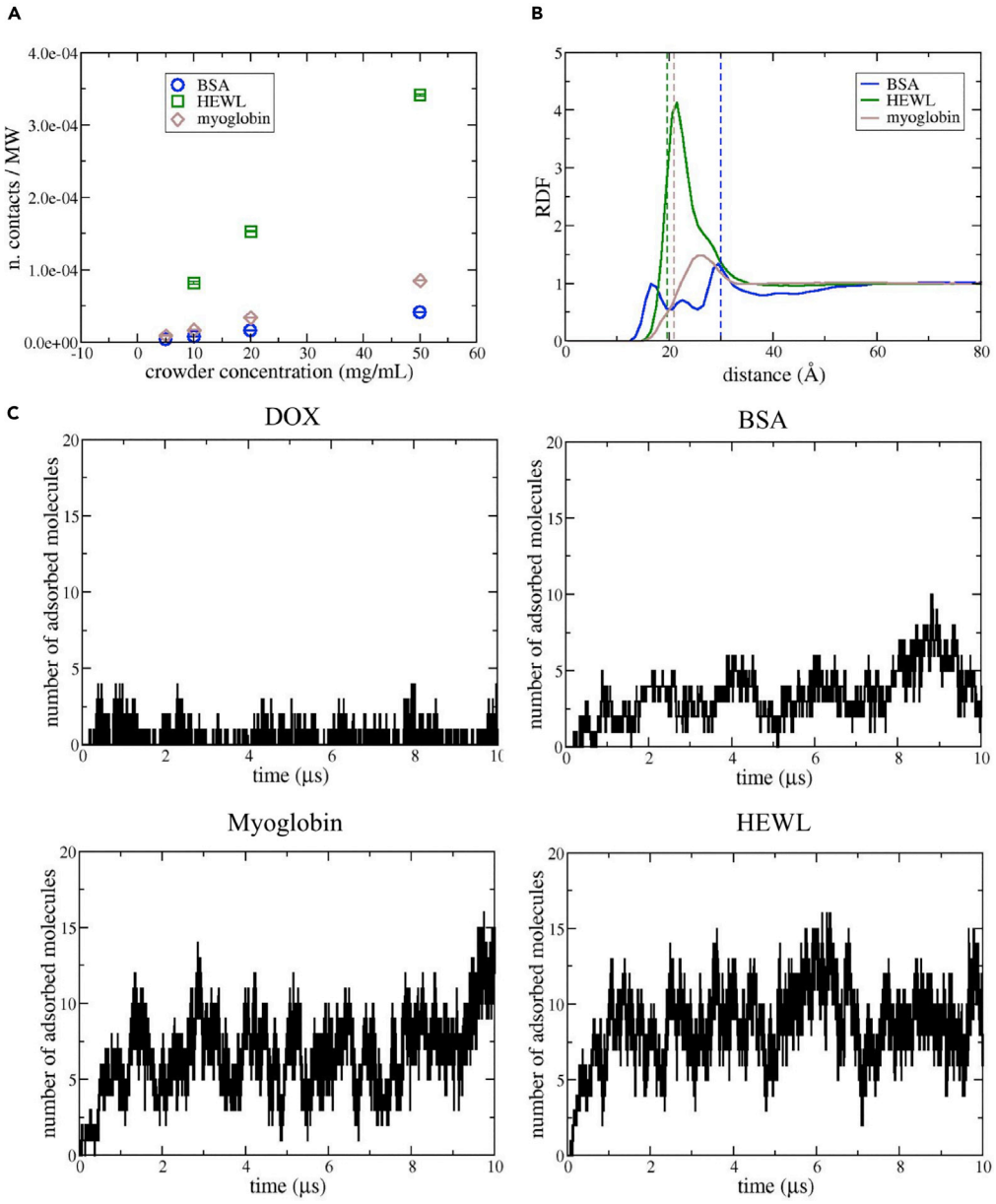

Figure 4. BD simulations reveal protein-drug interactions, and protein or drug adsorption to a silica surface

Interactions between fluorescein and protein crowders in BD simulations show differences between the three protein crowders. The number of protein-fluorescein contact interactions and the RDF peak are higher in the presence of HEWL, indicating stronger interactions of fluorescein with this protein crowder.

(A) Number of protein-fluorescein contact interactions divided by the molecular weight (MW) of the protein crowder (66637, 17820 and 14331 g/mol for BSA, myoglobin and HEWL, respectively) plotted against protein crowder concentration.

(B) Radial distribution functions (RDF) for protein-fluorescein distances computed from simulations with 50 mg/mL of crowder (pH 7.2, ionic strength of 190 mM). The dashed lines indicate the sum of the Stokes radii of the protein crowder and of fluorescein. Stokes radii of proteins: 25.7 Å, 16.6 Å and 15.3 Å for BSA, myoglobin and HEWL, respectively. Stokes radius of fluorescein: 4.3 Å.

(C) Number of doxorubicin or protein crowder molecules adsorbed to a silica surface in BD simulations performed with one type of solute molecule (80 molecules of DOX or 440 molecules of protein crowder at 50 mg/mL concentration, pH 7.2, ionic strength of 190 mM). Each plot shows results from a single BD simulation performed for 10 μs. The region adjacent to the surface was initially depleted of solute molecules (see STAR Methods for details). The silica surface is negatively charged and thus electrostatic interactions favor the binding of HEWL (+8 e) relative to BSA (−16 e).

of the other two protein crowders, without pre-coating the glass slides (when fluorescein can interact with the slower diffusing HEWL on the glass surface). The stronger interaction between fluorescein and HEWL can be explained by the strong electrostatic interaction between them, because at the pH of the experiments (7.4), fluorescein is negatively charged (-2 e) and HEWL is positively charged (+8 e). Another factor that contributes to this strong electrostatic interaction is the distribution of the molecular electrostatic potential of HEWL, which has a large positively charged region on the surface that interacts mostly with fluorescein during the BD simulations (Figure S5). Despite their negative net charges, myoglobin (-2 e) and BSA (−16 e) can also make favorable electrostatic interactions with fluorescein through regions of positive electrostatic potential on their surfaces and these are the parts of the protein surface with the greatest occupation of contacts with fluorescein during the BD simulations (Figure S5). However, these interactions are weaker than for HEWL and result in fewer contacts and much less pronounced peaks in the RDF (Figures 4, S6, and S7).

In summary, both experiments and simulations show that fluorescein makes contacts with all three crowders, with the highest number of contacts observed for binding to HEWL. This results in a modest reduction of the diffusion rates. However, the three proteins are adsorbed to the glass surface, with HEWL being the strongest adsorbed. This results in further reduction in fluorescein diffusion rates, as fluorescein interacts both with the immobile (surface adsorbed) and the mobile (in solution) protein molecules, with the reduction being greatest in the presence of HEWL.

Doxorubicin

The chemical structure and spectroscopic properties of DOX (MW = 580 Da) are shown in Figure 1B. It diffuses surprisingly slowly in PBS buffer, with $D_{confocal}$~ 12.6 $\mu m^2 s^{-1}$ (Figure 5A), whereas the infinite dilution translational diffusion coefficient of DOX (Stokes radius of 5.1 Å), D_{trans}, is calculated to be 412 $\mu m^2 s^{-1}$ (Table S2). Next, we measured the diffusion of DOX in DMSO, where $D_{confocal}$ increased to 47 $\mu m^2 s^{-1}$ (Figure 5A). Addition of 0.1% Tween 20 surfactant, which promotes the solubilization of aggregated hydrophobic DOX molecules and prevents surface attachment (Curry et al., 2015), increased $D_{confocal}$ in PBS to 27 $\mu m^2 s^{-1}$, with a similar value measured with 10 mg/mL BSA, with or without Tween 20 (Figure 5A). Micrographs of DOX in different solutions (Figure 5A, right panel) do not show obvious high MW aggregates. However, this does not exclude that DOX forms lower MW aggregates, as has been suggested previously (Fülöp et al., 2013), and could explain the slow diffusion of DOX in PBS. To further verify the $D_{confocal}$ values, we measured them after 10 and 63 ms bleach times. The corresponding recovery curves and bleach sizes are shown in Figure S8. The data clearly show much slower recovery curves after 63 ms bleach, which are accompanied by a wider bleach radius. However, the $D_{confocal}$ values calculated from $\tau_{1/2}$ and r_e were similar for the different bleach times (Table S3), in line with what we have previously found for protein diffusion (Dey et al., 2021).

Next, we measured DOX diffusion after addition of different concentrations of BSA or myoglobin (measurements with HEWL crowders were not possible as DOX precipitated on addition of HEWL). The addition of these proteins increased $D_{confocal}$ values up to ~40 $\mu m^2 s^{-1}$ (Figures 5C and 5D), close to the value recorded in DMSO (Figure 5A). Titration of increasing concentrations of BSA, from 0.01 to 200 mg/mL, showed that the maximum diffusion coefficient is reached at 10–20 mg/mL, with a decrease observed at higher BSA concentrations. This reduction can be associated with the excluded volume effect, which starts to be significant for BSA at the higher concentrations measured (fraction of occupied volume of 0.035 at 50 mg/mL BSA and 0.14 at 200 mg/mL BSA). BD simulations (which include intermolecular forces as well as excluded volume effects) show that not only the diffusion coefficient of DOX, but also that of BSA itself, is reduced as BSA concentrations increase from 20 to 200 mg/mL (Figures S4 and S9), in agreement with the experimental results.

Next, we determined the binding of DOX to BSA and myoglobin by fluorescence quenching titration experiments (Figures 5F, 5G, S3D, and S3E). BSA and myoglobin bind DOX with low affinities of 16.5 $\pm$ 2.5 μM and 18.4 $\pm$ 3.1 μM, respectively (Figures 5F, 5G and Table S1), in agreement with a previous study (Agudelo et al., 2012).

To investigate whether the slow diffusion of DOX in PBS is a result of surface attachment or self-aggregation, we determined the fluorescence intensity as a function of the distance from a glass surface for DOX. Whereas for fluorescein, we saw a homogeneous distribution of the small molecule in the drop, for DOX,

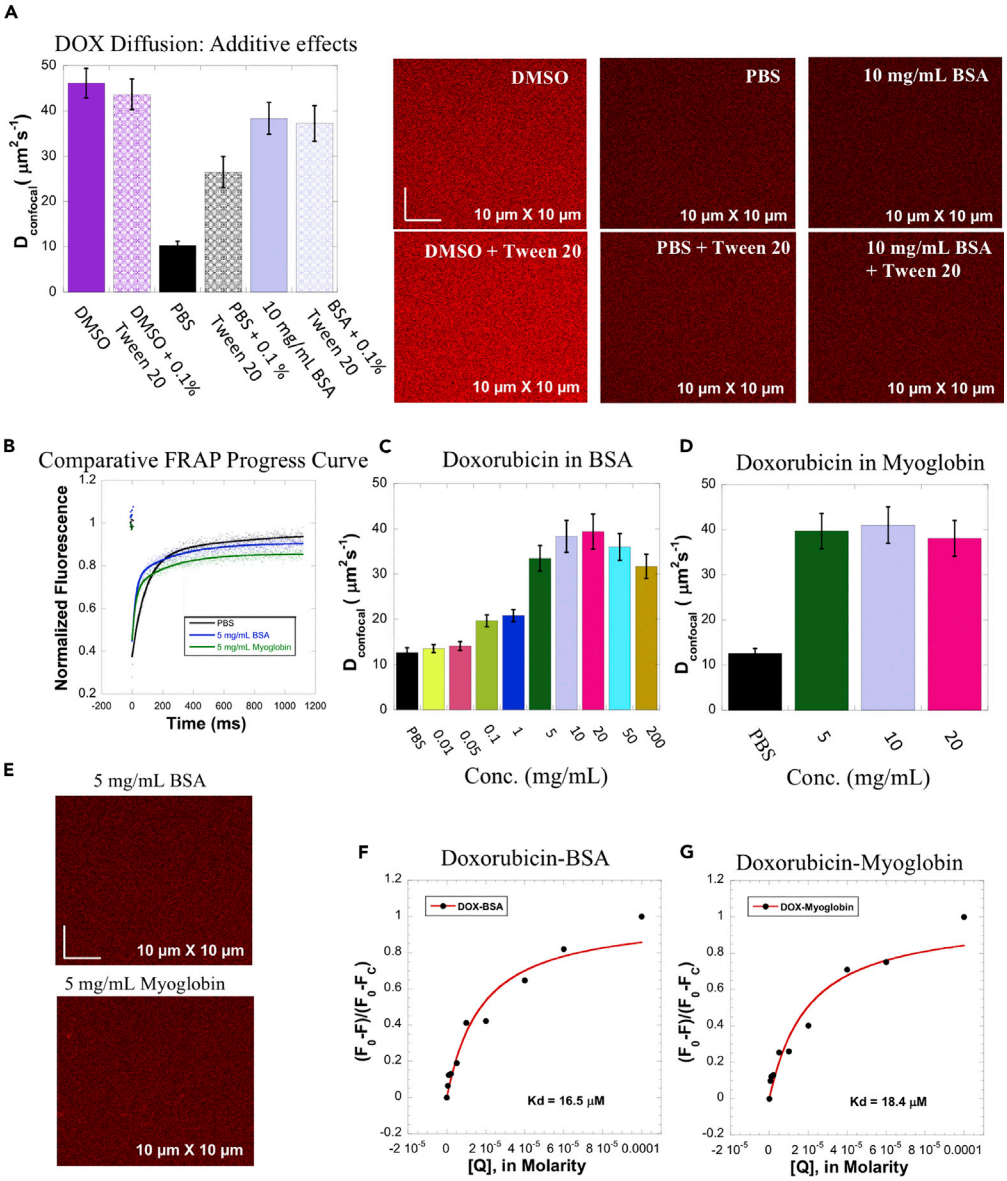

Figure 5. Doxorubicin diffusion in the presence of protein crowders

(A) Diffusion coefficients and images from confocal microscope of doxorubicin in DMSO, PBS or BSA solutions with or without Tween 20.

(B) Averaged FRAP profiles (N= 30; R= 0.99 for each of the fits) in PBS and in the presence of 5 mg/mL BSA and 5 mg/mL myoglobin.

(C and D) Diffusion coefficients of DOX in increasing amounts of (C) BSA and (D) myoglobin.

(E) Confocal microscopy images of doxorubicin in the presence of 5 mg/mL BSA and 5 mg/mL myoglobin.

(F and G) The results of binding affinity measurements showing $(F_0\text{-}F)/(F_0\text{-}F_c)$ versus [Q] plots from fluorescence quenching experiments of (F) DOX-BSA (R= 0.98), (G) DOX-myoglobin (R= 0.97) systems in PBS, where Q is the titrating drug concentration in molarity. Error bars represent SE calculated from fitting the FRAP progression curves, which are averaged over at least 30 independent measurements (see STAR methods).

surface attachment was clearly observed (Figure 3C). This is in line with a previous report that DOX can adsorb to a polypropylene surface (Curry et al., 2015). We then used BSA, myoglobin and PEG8000 solutions to coat the glass surface and thereby decrease the surface attachment and adsorption of the DOX molecules. Out of the three, myoglobin acted as the best surface coating agent for DOX molecules (Figure 3C), resulting in almost complete removal of DOX from the surface. In addition, myoglobin coating

of the glass surface resulted in a large increase in $D_{confocal}$ compared to DOX in PBS solution (Figure 3E), giving a value of 36 $\mu m^2 s^{-1}$, which is similar to the maximum value measured in the presence of BSA. The effect of BSA or PEG8000 coating of the glass surface on the $D_{confocal}$ values was minimal and DOX remained attached to the glass surface even after coating (Figures 3C and 3E). BD simulations in the absence of a surface show a low number of DOX-protein contacts (Figure S6) and small, broad RDF peaks for DOX-protein distances (Figure S7). This agrees with the experimental results, which show that the main effect of the protein crowders, especially at low concentrations, is prevention of DOX attachment to the glass surface, rather than slowed diffusion by quinary interactions with protein crowders, as observed for fluorescein. Nonetheless, it should be noted that quinary interactions between DOX and BSA are expected, as reported in a previous study (Agudelo et al., 2012).

BD simulations performed with a silica surface to mimic the glass plate and DOX molecules or the protein crowders at a concentration of 50 mg/mL show that all these types of molecules can adsorb to the negatively charged silica surface (Figure 4C), in agreement with previous studies using simulations or experiments (Kubiak-Ossowska et al., 2015, 2017; Romanowska et al., 2015; Diéz Fernández et al., 2020). However, a higher number of myoglobin and HEWL molecules adsorbed to the surface compared to DOX and BSA, indicating that myoglobin and HEWL interact better with the surface and may be better at preventing DOX surface attachment, consistent with the experimental results observed for DOX with myoglobin and BSA crowders. Measuring diffusion of DOX in PBS solution with an increased ionic strength (1000 mM NaCl) resulted in $D_{confocal}$ of 12.5 $\mu m^2 s^{-1}$ (Figure 3E), suggesting that the electrostatic attraction of the positively charged DOX to the negatively charged glass surface is not required for surface adsorption which is instead driven by hydrophobic interactions, in line with a previous report of DOX adsorption to polypropylene surfaces (Curry et al., 2015).

GSK3 inhibitor SB216763

GSK3 is a protein kinase that is active in a number of central intracellular signaling pathways, including cellular proliferation, migration, glucose regulation, and apoptosis (Coghlan et al., 2000). The GSK3 inhibitor SB216763 is currently being evaluated for several related malignancies (Coghlan et al., 2000). The chemical structure and spectroscopic properties of SB216763 are shown in Figure 1C. SB216763 has a strong tendency to aggregate in PBS (Figure 6A). Aggregation is also observed in DMEM media. Of the four small molecules tested, the GSK3 inhibitor is the only one with neutral net charge at the pH of the experiments. The lack of repulsive electrostatic interactions and the high hydrophobicity (indicated by a logP value of 4.5, Figure 1C) may facilitate aggregation. Moreover, BD simulations of the GSK3 inhibitor without protein crowders showed greater self-interactions than those observed for the other small molecules (Table S4), consistent with the experimental data. The addition of BSA (but not HEWL or myoglobin) eliminates the aggregation, especially at concentrations of 25 and 50 mg/mL (Figure 6A). FRAP experiments validate the micrograph observations (Figures 6B–6E). The percent FRAP recovery of SB216763 is very low in buffer or in the presence of myoglobin crowders, but reaches close to 100% with the addition of 50 mg/mL BSA (see normalized fluorescence in Figure 6B). Also, $D_{confocal}$ is much higher in the presence of 50 mg/mL BSA (Figure 6C). FRAP recovery is in line with the micrographs shown in Figure 6A. Titrating increasing concentrations of BSA into SB216763 solutions shows $D_{confocal}$ values increasing to 15 $\mu m^2 s^{-1}$ in the presence of 10 mg/mL BSA and to 25 $\mu m^2 s^{-1}$ in the presence of 100 mg/mL BSA. These $D_{confocal}$ values are consistent with solubilization of high molecular weight aggregates of SB216763. Interestingly, binding experiments of SB216763 to BSA, HEWL, and myoglobin showed affinities of 5.2 $\pm$ 1.2 μM, 1.7 $\pm$ 0.7 μM, and 7.3 $\pm$ 1.8 μM, respectively (Figures 6G–6I and Table S1). Thus, although BSA solubilizes SB216763 much better than the other two proteins, we did not find a relation between solubilization of the small molecule and binding affinity.

Visual inspection of the apo and holo crystal structures of the protein crowders shows that myoglobin does not have a crevice or buried binding site for small molecules larger than molecular oxygen, whereas HEWL and BSA do. Moreover, HEWL and BSA were shown to bind to small molecules and act as potential drug carriers (Agudelo et al., 2012; Fliszár-Nyúl et al., 2019; Nassab et al., 2021). HEWL can accommodate small molecules in the crevice of its catalytic site, whereas BSA has four binding cavities that can accommodate small molecules (Figure 6F). Docking of SB216763 to BSA and to HEWL shows that the GSK3 inhibitor can bind to one of the cavities of BSA with a good docking score (−9.2 kcal/mol, Figure 6F) and to the catalytic site of HEWL with a less favorable docking score (−7.9 kcal/mol). The deep binding cavities in BSA that can accommodate SB216763 may explain why BSA is the only protein crowder that can reduce the aggregation

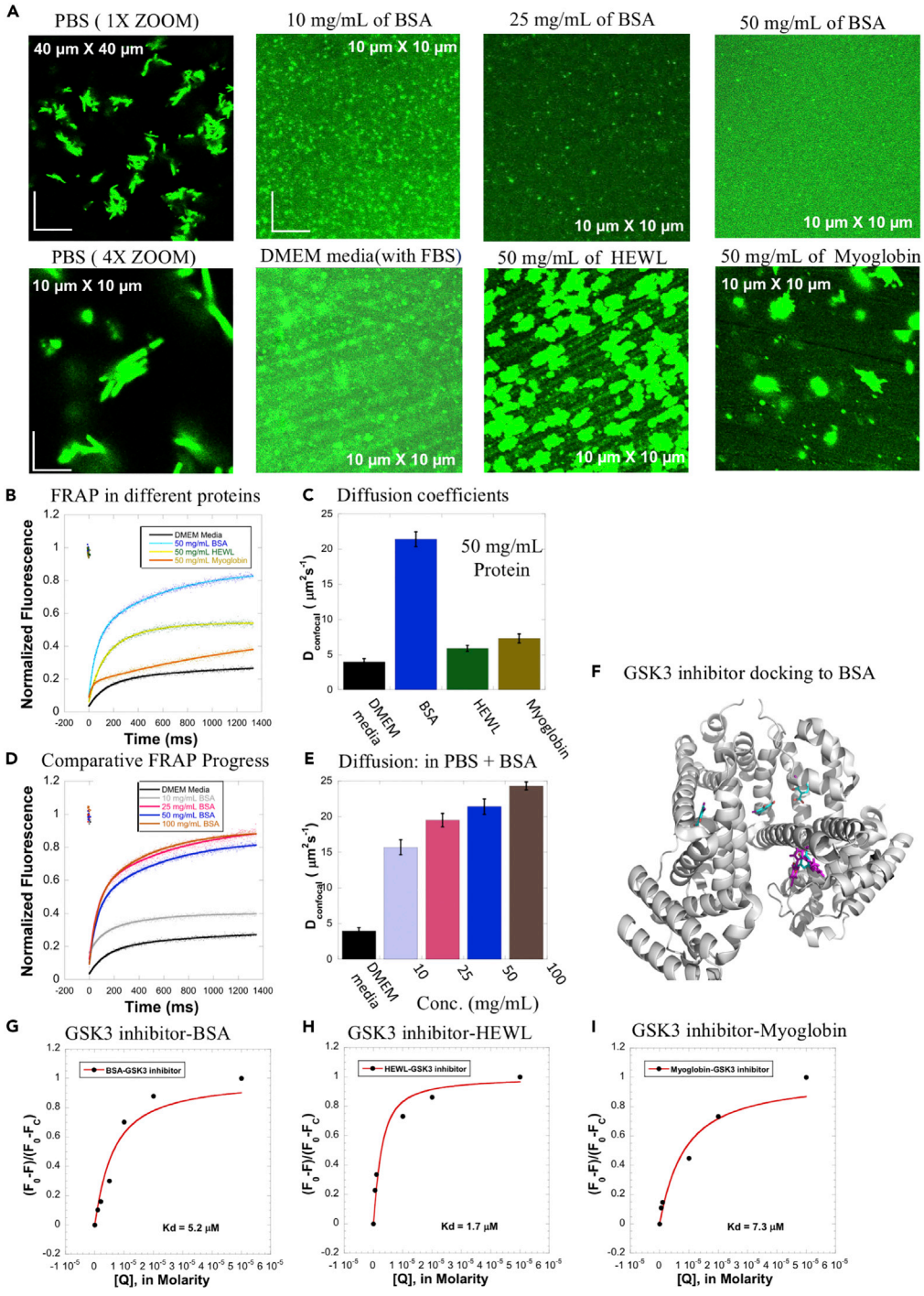

Figure 6. GSK3 inhibitor diffusion in the presence of protein crowders

(A) Confocal images of GSK3 inhibitor aggregates in PBS, DMEM media, BSA, HEWL and myoglobin. Note the disappearance of aggregation with increasing BSA concentration.

(B) Averaged FRAP profiles (N = 30; R = 0.99 for each of the fits) and (C) diffusion coefficients for GSK3 inhibitor in the presence of 50 mg/mL BSA, HEWL and myoglobin.

(D) Averaged FRAP profiles (N = 30; R = 0.99 for each of the fits) and (E) diffusion coefficients of GSK3 inhibitor in different concentrations of BSA protein.

(F) BSA (gray) bound to 3,5-diiodosalicylic acid (PDB 4JK4, ligand with carbons in cyan). Docking of the GSK3 inhibitor (pink) to BSA (PDB 4F5S) was performed using different grid centers to capture each of the four binding sites for

Figure 6. *Continued*
3,5-diiodosalicylic acid. In one of the binding sites, the GSK3 inhibitor occupied a position similar to that of 3,5-diiodosalicylic acid, showing that the GSK3 inhibitor can bind to a rather buried binding site on BSA.
(G–I): $(F_0\text{-}F)/(F_0\text{-}F_c)$ versus [Q] plots from fluorescence quenching experiments of GSK3 inhibitor-BSA (R= 0.97)/HEWL (R= 0.98)/myoglobin (R= 0.98) systems in PBS buffer, where Q is the titrating drug concentration in molarity.
Error bars represent SE calculated from fitting the FRAP progression curves, which are averaged over at least 30 independent measurements (see STAR methods).

of this small molecule. The diffusion coefficients computed from BD simulations did not show the trends obtained experimentally for SB216763 in the presence of protein crowders (Figure S4), indicating the importance of factors omitted in the BD model, such as small molecule aggregation and binding of small molecules within rather buried cavities in the protein crowder.

Quinacrine dihydrochloride

Quinacrine dihydrochloride (MW= 472.9 Da), whose chemical structure and spectroscopic properties are shown in Figure 1D, is among the first antimalarial drugs discovered. Recently, it was also suggested to have high potency against SARS-CoV-2 in an *in vitro* setting (Rojas et al., 2021). Quinacrine does not display any significant aggregation issues in buffer solutions (Figures 7A and 7B), and it is not adsorbed onto glass surfaces (Figure 3D). The addition of BSA, HEWL or myoglobin did not affect its diffusion coefficient ($D_{confocal}\sim$ 41–43 $\mu m^2 s^{-1}$, Figures 7C and 7D). Control experiments in DMSO and in other media with and without the presence of Tween 20 did not alter the $D_{confocal}$ values significantly, consistent with the observed solubility of quinacrine across multiple solutions (Figure 7A). Measuring the binding affinity of quinacrine to BSA, HEWL and myoglobin showed affinities of 4.6 $\pm$ 1.1 μM, 4.7 $\pm$ 0.8 μM and 3.0 $\pm$ 0.4 μM, respectively (Figures 7E–7G and Table S1).

As in the experiments, diffusion coefficients computed from BD simulations for quinacrine show no significant difference on adding 50 mg/mL protein crowder (Figure S4). One reason for the insensitivity to protein crowders is that quinacrine-protein contacts are less prominent compared to the other small molecules in BD simulations (Figure S6), as also shown by the absence of a peak in the quinacrine-HEWL RDF (Figure S7). However, the number of quinacrine-protein contacts was similar to that for the other small molecules for myoglobin and contacts were more pronounced for BSA. These differences are consistent with the larger positive charge on quinacrine than the other molecules (+2 e), resulting in greater solubility in aqueous solution and a net charge repulsion to HEWL and a net charge attraction to BSA, which however does not result in any significant difference in either the computed or the experimentally determined diffusion coefficients for quinacrine in 50 mg/mL BSA.

DISCUSSION

Studying the diffusion of low MW drugs in diverse environments is challenging, mostly because only a few drugs have the desired spectral properties. Nevertheless, studying their behavior in aqueous solution and in the presence of macromolecular crowders is important as these environments are relevant for their administration and action. Here, we measured the diffusion of the four molecules in buffer solutions and solutions containing one of three different proteins as crowders, BSA, HEWL, and myoglobin. In addition, we determined the affinity of the small molecules for the three proteins using fluorescence quenching. The equilibrium dissociation constants are moderate (in the range of 1–100 μM). These moderate affinities explain the lack of co-elution in size exclusion chromatography (SEC) of the small molecules to the protein crowders (Figures S10, S11, and S12). Co-elution can be observed only for binding affinities better than 0.1 μM, which is not the case here. Yet, the addition of the proteins had a substantial effect on the diffusion of the small molecules. BD simulations and molecular docking revealed mechanistic details of the main experimental observations, providing further evidence for the different mechanisms of modulation of small molecule diffusion rates observed for the four compounds.

Each of the four small molecules studied behaved differently, providing excellent examples for different types of diffusional behavior of small molecules (Figure 8). Quinacrine dihydrochloride is a cationic charged, water-soluble compound. Its measured diffusion rate is not affected by the glass surface or the protein crowders. Fluorescein is a negatively charged, water-soluble compound. It forms interactions with proteins, which slow down its diffusion, mostly through its interaction with the surface adsorbed fraction of the proteins (Figures 3A, 3B, and 4). The opposite is observed for DOX, a positively charged

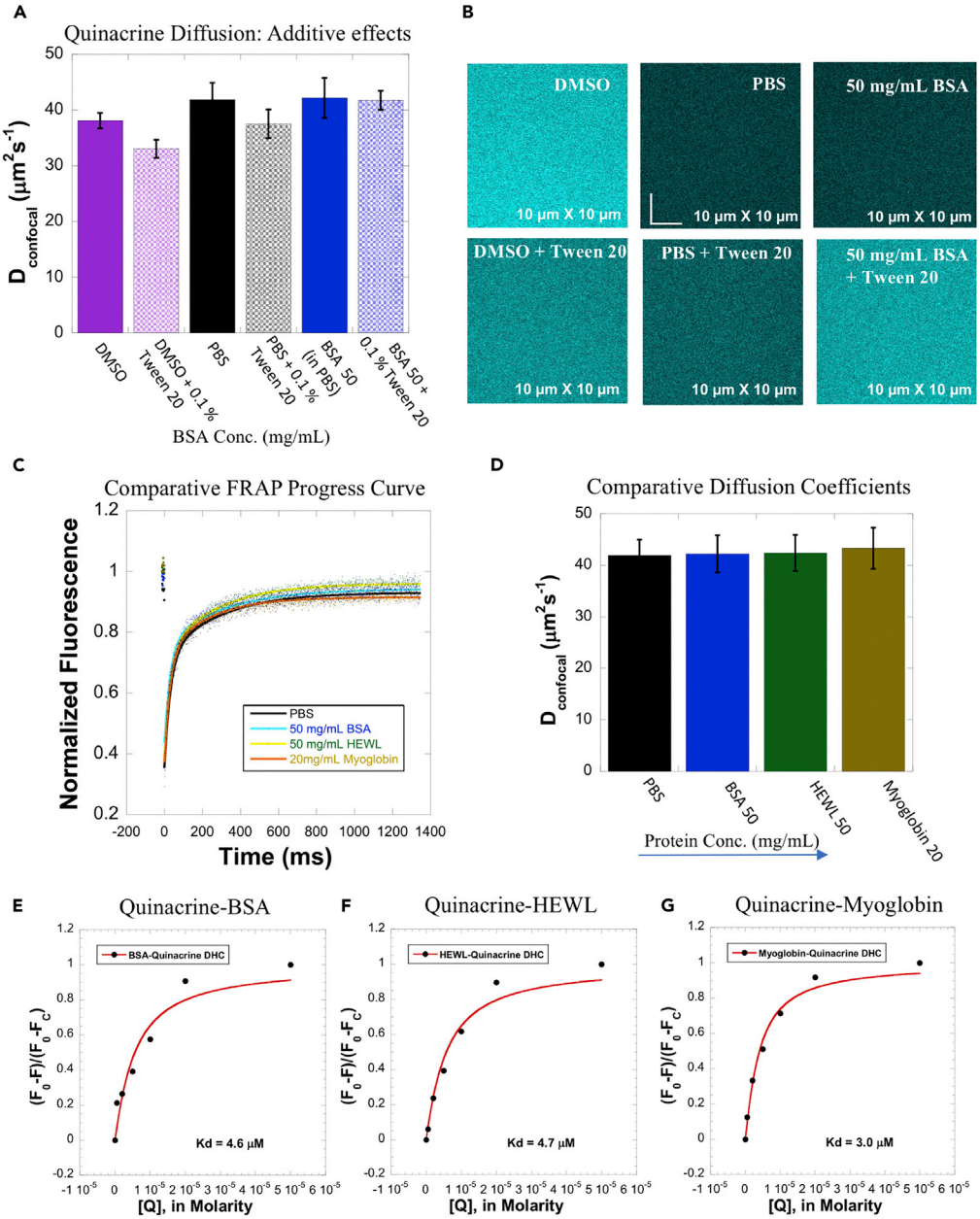

Figure 7. Quinacrine in the presence of protein crowders

(A and B) Comparative (A) diffusion coefficients and (B) images from confocal microscope of quinacrine DHC in diversified environments with or without presence of tween 20 are shown.

(C–G) (C) Comparative averaged FRAP profiles (R = 0.99 for each of the fits) and (D) comparative diffusion coefficients of quinacrine DHC in presence of 50 mg/mL of BSA, HEWL, 20 mg/mL of Myoglobin and PBS buffer only are shown. $(F_0\text{-}F)/(F_0\text{-}F)$ versus [Q] plots from fluorescence quenching experiments of Quinacrine DHC-BSA (R= 0.97)/HEWL (R= 0.99)/ Myoglobin (R= 0.99) system in PBS buffer is shown in (E–G), where Q is the titrating drug concentration in Molarity. Error bars represent SE calculated from fitting the FRAP progression curves, which are averaged over at least 30 independent measurements (see STAR methods).

molecule, which diffuses slowly in PBS, but at a faster rate on the addition of protein crowders. A detailed analysis showed that DOX adsorbs to the glass surface and this is the reason for the slow diffusion. Last, SB216763 is a molecule with neutral net charge that is insoluble in water and forms large aggregates. However, addition of BSA as a carrier protein solubilizes SB216763, as observed from micrographs,

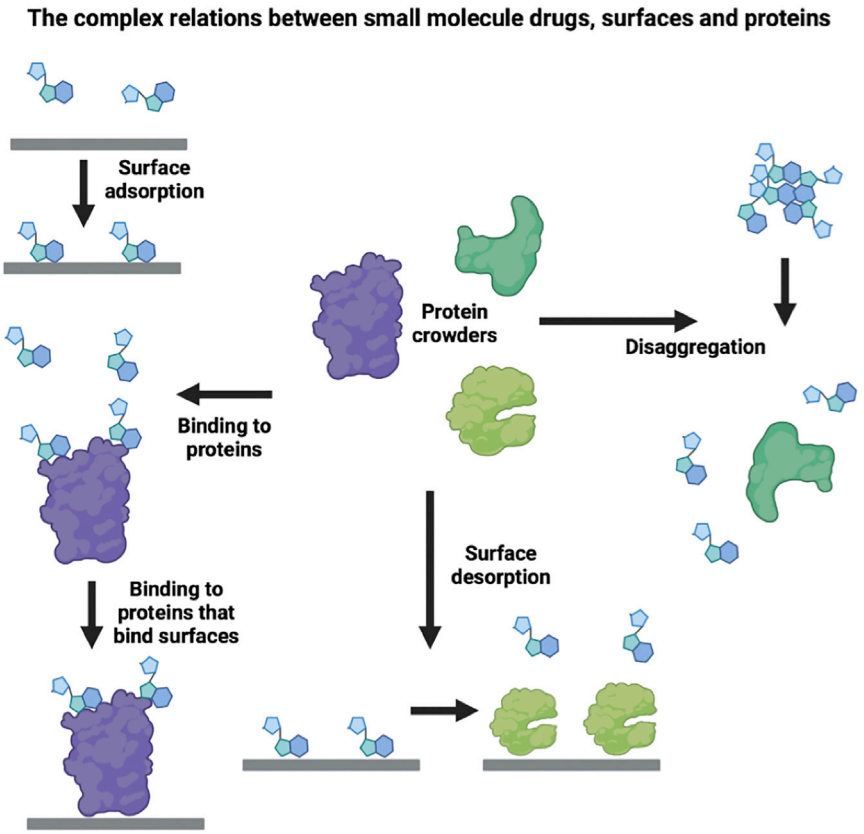

Figure 8. Effects of protein crowders and surfaces on the diffusion of small molecules

The effects of protein crowders go beyond the slower diffusion because of excluded volume. Here, we find that the diffusion coefficients can be decreased because of surface adsorption or binding to proteins that are adsorbed on the surface. On the other hand, diffusion coefficients can be increased by surface desorption or disaggregation of the small molecules. The specific effect of the protein crowder on the diffusion coefficient of the small molecule depends on the physicochemical properties of the crowder and of the small molecule – which influence the protein-small molecule, protein-(glass) surface and small-molecule-surface interactions, as well as self-interactions.

the fraction of recovery, the increased diffusion rate, and its ability to bind in a rather buried binding site on BSA.

Overall, out of the 4 molecules analyzed, 3 exhibited non-standard diffusional behavior. Up to the highest protein crowder concentrations studied in BD simulations and FRAP experiments (50 mg/mL), sub-diffusion of the small molecules was not observed in BD simulations, because the curves of mean square displacement could be well-fitted with a linear equation (Figure S13). Moreover, in previous BD simulations of solutions crowded with the proteins myoglobin and hemoglobin (up to protein concentrations of 550 mg/mL), sub-diffusion was not observed for the proteins (Mereghetti and Wade, 2012). In addition, the viscosity of 10 and 50 mg/mL BSA solutions is only 1.015 mPas and 1.2 mPas respectively (Yadav et al., 2011), too low to show the effects observed here. Conversely, the diffusion of two of these three molecules was affected by surface interactions: DOX interacted directly with the surface, whereas fluorescein interacted indirectly with the surface. These surface interactions can influence drug quantification, causing systematic errors in the amount delivered, and they also indicate potential interactions in a physiological environment, such as with blood vessel surfaces, cell membranes or with artificial implants. Although these were not investigated here, our findings call for a better evaluation of such direct and indirect surface interactions.

In summary, by combining experiments and simulations, we observe that the effects of protein crowders on the diffusion of low molecular weight drug molecules go beyond the slowing of translational diffusion because of excluded volume, and find that the diffusion of drugs can also be slowed down because of

quinary interactions, with the extent dependent on protein-surface interactions, or it can be increased by surface detachment or a reduction in aggregation of the small molecules (Figure 8).

Limitation of the study

A point of potential concern is the "slow" measured diffusion coefficients for the small molecules, which are much below those expected for these molecules in aqueous solution. A possible reason could be limitations in the Line-FRAP method, which may not allow the measurement of high diffusion coefficients (>100 $\mu m^2 s^{-1}$). If this would be a result of a "dead-time" between the end of the bleach and the first recovery data points, we should observe an incomplete bleach (as some recovery occurs before the first data measurement). However, the FRAP curves in Figures 2, 5, 6, and 7 do not show reduced bleach, even for the fastest diffusing molecules. This would suggest that for fast diffusing particles, the data analysis carried out on the experimental observations does not provide absolute diffusion coefficients. Therefore, we name the derived values $D_{confocal}$. However, we consider the relative diffusion rates between the different conditions applied in this study to be robust, as the same data analysis procedure was carried out for all conditions. Unfortunately, methods such as FCS, which could provide an orthogonal approach for diffusion measurements, are not applicable to the small molecules used here, because of their low quantum yield. Thus, this study was limited to a maximum protein crowder concentration of 50 mg/mL, which is lower than the physiological protein crowder concentration of 200–300 mg/mL. It should also be noted that the protein crowders and small molecules were treated as rigid bodies in the BD simulations, preventing the complete representation of effects dependent on molecular flexibility which were later identified as important in the experiments, like small molecule aggregation and the binding of small molecules to buried cavities in proteins.

STAR★METHODS

Detailed methods are provided in the online version of this paper and include the following:

- KEY RESOURCES TABLE
- RESOURCE AVAILABILITY
  - Lead contact
  - Materials availability
  - Data and code availability
- EXPERIMENTAL MODEL AND SUBJECT DETAILS
- METHOD DETAILS
  - Confocal microscopy and FRAP analysis
  - Line-FRAP and classical XY-FRAP
  - Steady-state fluorescence quenching assays
  - Dynamic light scattering (DLS) measurements
  - Size exclusion chromatography
  - Brownian dynamics simulations
  - Computation of diffusion coefficients for small molecules
  - Docking of the small molecules to the proteins
- QUANTIFICATION AND STATISTICAL ANALYSIS
  - Calculating diffusion rates and statistical analysis

SUPPLEMENTAL INFORMATION

Supplemental information can be found online at https://doi.org/10.1016/j.isci.2022.105088.

ACKNOWLEDGMENTS

We gratefully acknowledge Stefan Richter (HITS) for technical support of the computational work, Neil J. Bruce (HITS), Daria B. Kokh (HITS) and Huan-Xiang Zhou (University of Illinois at Chicago) for helpful discussions, and Gaurav Ganotra (HITS) for help with the parameterization of small molecules. This work was supported by the Israel Science Foundation grant no. 1268/18 (GS), a Capes-Humboldt postdoctoral scholarship to AN-A (Capes process number 88881.162167/2017-01), funds from the Cluster of Excellence CellNetworks (DFG, EXC81) to AN-A, the European Union's Horizon 2020 Framework Programme for Research and Innovation under Grant Agreements 785907 and 945539 (Human Brain Project SGA2 and SGA3) (RCW), and the Klaus Tschira Foundation (AN-A, RCW).

AUTHOR CONTRIBUTIONS

D.D. carried out the experiments. A.N.-A. performed the computer simulations. D.D., A.N.-A., R.C.W., and G.S. conceived the study, analyzed the data and wrote the manuscript.

DECLARATION OF INTERESTS

The authors declare no competing interests.

Received: June 17, 2022
Revised: August 4, 2022
Accepted: August 31, 2022
Published: October 21, 2022

REFERENCES

Agudelo, D., Bourassa, P., Bruneau, J., Bérubé, G., Asselin, É., and Tajmir-Riahi, H.A. (2012). Probing the binding sites of antibiotic drugs doxorubicin and N-(trifluoroacetyl) doxorubicin with human and bovine serum albumins. PLoS One *7*, e43814. https://doi.org/10.1371/journal.pone.0043814.

Axelrod, D., Koppel, D.E., Schlessinger, J., Elson, E., and Webb, W.W. (1976). Mobility measurement by analysis of fluorescence photobleaching recovery kinetics. Biophys. J. *16*, 1055–1069. https://doi.org/10.1016/S0006-3495(76)85755-4.

Balbo, J., Mereghetti, P., Herten, D.P., and Wade, R.C. (2013). The shape of protein crowders is a major determinant of protein diffusion. Biophys. J. *104*, 1576–1584. https://doi.org/10.1016/j.bpj.2013.02.041.

Bayly, C.I., Cieplak, P., Cornell, W., and Kollman, P.A. (1993). A well-behaved electrostatic potential based method using charge restraints for deriving atomic charges: the RESP model. J. Phys. Chem. *97*, 10269–10280. https://doi.org/10.1021/j100142a004.

Bujacz, A. (2012). Structures of bovine, equine and leporine serum albumin. Acta Crystallogr. D Biol. Crystallogr. *68*, 1278–1289. https://doi.org/10.1107/S0907444912027047.

Bullerjahn, J.T., von Bülow, S., and Hummer, G. (2020). Optimal estimates of self-diffusion coefficients from molecular dynamics simulations. J. Chem. Phys. *153*, 024116. https://doi.org/10.1063/5.0008312.

Carvalho, C., Santos, R.X., Cardoso, S., Correia, S., Oliveira, P.J., Santos, M.S., and Moreira, P.I. (2009). Doxorubicin: the good, the bad and the ugly effect. Curr. Med. Chem. *16*, 3267–3285. https://doi.org/10.2174/092986709788803312.

Case, D.A., Betz, R.M., Cerutti, D.S., Darden, T.A., Duke, R.E., Giese, T.J., Gohlke, H., Goetz, A.W., Homeyer, N., et al. (2016). Amber16 (University of California). https://doi.org/10.13140/RG.2.2.27958.70729.

Chu, K., Vojtchovský, J., McMahon, B.H., Sweet, R.M., Berendzen, J., and Schlichting, I. (2000). Structure of a ligand-binding intermediate in wild-type carbonmonoxy myoglobin. Nature *403*, 921–923. https://doi.org/10.1038/35002641.

Coghlan, M.P., Culbert, A.A., Cross, D.A., Corcoran, S.L., Yates, J.W., Pearce, N.J., Rausch, O.L., Murphy, G.J., Carter, P.S., Roxbee Cox, L., et al. (2000). Selective small molecule inhibitors of glycogen synthase kinase-3 modulate glycogen metabolism and gene transcription. Chem. Biol. *7*, 793–803. https://doi.org/10.1016/S1074-5521(00)00025-9.

Cornell, W.D., Cieplak, P., Bayly, C.I., and Kollman, P.A. (1993). Application of RESP charges to calculate conformational energies, hydrogen bond energies, and free energies of solvation. J. Am. Chem. Soc. *115*, 9620–9631. https://doi.org/10.1021/ja00074a030.

Curry, D., Scheller, H., Lu, M., Mkandawire, M., Servos, M.R., Cui, S., Zhang, X., and Oakes, K.D. (2015). Prevention of doxorubicin sorptive losses in drug delivery studies using polyethylene glycol. RSC Adv. *5*, 25693–25698. https://doi.org/10.1039/c5ra01799h.

Dauty, E., and Verkman, A.S. (2004). Molecular crowding reduces to a similar extent the diffusion of small solutes and macromolecules: measurement by fluorescence correlation spectroscopy. J. Mol. Recognit. *17*, 441–447. https://doi.org/10.1002/jmr.709.

Deschout, H., Raemdonck, K., Demeester, J., de Smedt, S.C., and Braeckmans, K. (2014). FRAP in pharmaceutical research: practical guidelines and applications in drug delivery. Pharm. Res. (N. Y.) *31*, 255–270. https://doi.org/10.1007/s11095-013-1146-9.

Dey, D., Marciano, S., Nunes-Alves, A., Kiss, V., Wade, R.C., and Schreiber, G. (2021). Line-FRAP, A versatile method to measure diffusion rates in vitro and in vivo. J. Mol. Biol. *433*, 166898. https://doi.org/10.1016/j.jmb.2021.166898.

Di, L., Artursson, P., Avdeef, A., Ecker, G.F., Faller, B., Fischer, H., Houston, J.B., Kansy, M., Kerns, E.H., Krämer, S.D., et al. (2012). Evidence-based approach to assess passive diffusion and carrier-mediated drug transport. Drug Discov.Today *17*, 905–912. https://doi.org/10.1016/j.drudis.2012.03.015.

Díez Fernández, A., Charchar, P., Cherstvy, A.G., Metzler, R., and Finnis, M.W. (2020). The diffusion of doxorubicin drug molecules in silica nanoslits is non-Gaussian, intermittent and anticorrelated. Phys. Chem. Chem. Phys. *22*, 27955–27965. https://doi.org/10.1039/d0cp03849k.

Dobson, P.D., and Kell, D.B. (2008). Carrier-mediated cellular uptake of pharmaceutical drugs: an exception or the rule? Nat. Rev. Drug Discov. *7*, 205–220. https://doi.org/10.1038/nrd2438.

Dolinsky, T.J., Nielsen, J.E., McCammon, J.A., and Baker, N.A. (2004). PDB2PQR: an automated pipeline for the setup of Poisson-Boltzmann electrostatics calculations. Nucleic Acids Res. *32*, W665–W667. https://doi.org/10.1093/nar/gkh381.

Ehsanian, R., van Waes, C., and Feller, S.M. (2011). Beyond DNA binding - a review of the potential mechanisms mediating quinacrine's therapeutic activities in parasitic infections, inflammation, and cancers. Cell Commun. Signal. *9*, 13. https://doi.org/10.1186/1478-811X-9-13.

Feig, M., and Sugita, Y. (2012). Variable interactions between protein crowders and biomolecular solutes are important in understanding cellular crowding. J. Phys. Chem. B *116*, 599–605. https://doi.org/10.1021/jp209302e.

Feig, M., Nawrocki, G., Yu, I., Wang, P.H., and Sugita, Y. (2018). Challenges and opportunities in connecting simulations with experiments via molecular dynamics of cellular environments. J. Phys. Conf. Ser. *1036*, 012010. https://doi.org/10.1088/1742-6596/1036/1/012010.

Feng, B.Y., Simeonov, A., Jadhav, A., Babaoglu, K., Inglese, J., Shoichet, B.K., and Austin, C.P. (2007). A high-throughput screen for aggregation-based inhibition in a large compound library. J. Med. Chem. *50*, 2385–2390. https://doi.org/10.1021/jm061317y.

Fliszár-Nyúl, E., Lemli, B., Kunsági-Máté, S., Dellafiora, L., Dall'Asta, C., Cruciani, G., Pethő, G., and Poór, M. (2019). Interaction of mycotoxin alternariol with serum albumin. Int. J. Mol. Sci. *20*, 2352. https://doi.org/10.3390/ijms20092352.

Fülöp, Z., Gref, R., and Loftsson, T. (2013). A permeation method for detection of self-aggregation of doxorubicin in aqueous environment. Int. J. Pharm. *454*, 559–561. https://doi.org/10.1016/j.ijpharm.2013.06.058.

Gabdoulline, R.R., and Wade, R.C. (1996). Effective charges for macromolecules in solvent. J. Phys. Chem. *100*, 3868–3878. https://doi.org/10.1021/jp953109f.

Ganotra, G.K. (2020). Computational Studies of Drug-Binding Kinetics (Germany: Dissertation at Heidelberg University). https://doi.org/10.11588/heidok.00027374.

García De La Torre, J., Huertas, M.L., and Carrasco, B. (2000). Calculation of hydrodynamic properties of globular proteins from their atomic-level structure. Biophys. J. *78*, 719–730. https://doi.org/10.1016/S0006-3495(00)76630-6.

Giammona, D.A. (1984). An Examination of Conformational Flexibility in Porphyrins and Bulky-Ligand Binding in Myoglobin (University of California, Davis ProQuest Dissertations Publishing).

Gordon, M.S., and Schmidt, M.W. (2005). In Chapter 41 - Advances in electronic structure theory: GAMESS a decade later Theory and Applications of Computational Chemistry, C.E. Dykstra, G. Frenking, K.S. Kim, and G.E. Scuseria, eds. (Elsevier), pp. 1167–1189.

Gray, D.E. (1957). American Institute of physics handbook coordinating. Butsuri *12*, 381–383. https://doi.org/10.11316/butsuri1946.12.8.381.

Hoffmann, M., Wagner, C.S., Harnau, L., and Wittemann, A. (2009). 3D brownian diffusion of submicron-sized particle clusters. ACS Nano *3*, 3326–3334. https://doi.org/10.1021/nn900902b.

Huber, G.A., and McCammon, J.A. (2019). Brownian dynamics simulations of biological molecules. Trends Chem. *1*, 727–738. https://doi.org/10.1016/j.trechm.2019.07.008.

Kasahara, K., Re, S., Nawrocki, G., Oshima, H., Mishima-Tsumagari, C., Miyata-Yabuki, Y., Kukimoto-Niino, M., Yu, I., Shirouzu, M., Feig, M., and Sugita, Y. (2021). Reduced efficacy of a Src kinase inhibitor in crowded protein solution. Nat. Commun. *12*, 4099. https://doi.org/10.1038/s41467-021-24349-5.

Kekenes-Huskey, P.M., Eun, C., and McCammon, J.A. (2015). Enzyme localization, crowding, and buffers collectively modulate diffusion-influenced signal transduction: insights from continuum diffusion modeling. J. Chem. Phys. *143*, 094103. https://doi.org/10.1063/1.4929528.

Kubiak-Ossowska, K., Cwieka, M., Kaczynska, A., Jachimska, B., and Mulheran, P.A. (2015). Lysozyme adsorption at a silica surface using simulation and experiment: effects of pH on protein layer structure. Phys. Chem. Chem. Phys. *17*, 24070–24077. https://doi.org/10.1039/c5cp03910j.

Kubiak-Ossowska, K., Tokarczyk, K., Jachimska, B., and Mulheran, P.A. (2017). Bovine serum albumin adsorption at a silica surface explored by simulation and experiment. J. Phys. Chem. B *121*, 3975–3986. https://doi.org/10.1021/acs.jpcb.7b01637.

Lipinski, C.A., Lombardo, F., Dominy, B.W., and Feeney, P.J. (1997). Experimental and computational approaches to estimate solubility and permeability in drug discovery and development settings. Adv. Drug Deliv. Rev. *23*, 3–25. https://doi.org/10.1016/S0169-409X(96)00423-1.

Longsworth, L.G. (1953). Diffusion measurements, at 25°, of aqueous solutions of amino acids, peptides and sugars. J. Am. Chem. Soc. *75*, 5705–5709. https://doi.org/10.1021/ja01118a065.

Lorén, N., Hagman, J., Jonasson, J.K., Deschout, H., Bernin, D., Cella-Zanacchi, F., Diaspro, A., McNally, J.G., Ameloot, M., Smisdom, N., et al. (2015). Fluorescence recovery after photobleaching in material and life sciences: putting theory into practice. Q. Rev. Biophys. *48*, 323–387. https://doi.org/10.1017/S0033583515000013.

Manley, S., Gillette, J.M., Patterson, G.H., Shroff, H., Hess, H.F., Betzig, E., and Lippincott-Schwartz, J. (2008). High-density mapping of single-molecule trajectories with photoactivated localization microscopy. Nat. Methods *5*, 155–157. https://doi.org/10.1038/nmeth.1176.

Martinez, M., Bruce, N.J., Romanowska, J., Kokh, D.B., Ozboyaci, M., Yu, X., Öztürk, M.A., Richter, S., and Wade, R.C. (2015). SDA 7: a modular and parallel implementation of the simulation of diffusional association software. J. Comput. Chem. *36*, 1631–1645. https://doi.org/10.1002/jcc.23971.

Mereghetti, P., and Wade, R.C. (2012). Atomic detail brownian dynamics simulations of concentrated protein solutions with a mean field treatment of hydrodynamic interactions. J. Phys. Chem. B *116*, 8523–8533. https://doi.org/10.1021/jp212532h.

Miguel Rubi, J. (2019). Entropic diffusion in confined soft-matter and biological systems. EPL *127*, 10001. https://doi.org/10.1209/0295-5075/127/10001.

Miklos, A.C., Sarkar, M., Wang, Y., and Pielak, G.J. (2011). Protein crowding tunes protein stability. J. Am. Chem. Soc. *133*, 7116–7120. https://doi.org/10.1021/ja200067p.

Miyamoto, S., and Shimono, K. (2020). Molecular modeling to estimate the diffusion coefficients of drugs and other small molecules. Molecules *25*, 5340. https://doi.org/10.3390/molecules25225340.

Nassab, C.N., Arooj, M., Shehadi, I.A., Parambath, J.B.M., Kanan, S.M., and Mohamed, A.A. (2021). Lysozyme and human serum albumin proteins as potential nitric oxide cardiovascular drug carriers: theoretical and experimental investigation. J. Phys. Chem. B *125*, 7750–7762. https://doi.org/10.1021/acs.jpcb.1c04614.

O'Boyle, N.M., Banck, M., James, C.A., Morley, C., Vandermeersch, T., and Hutchison, G.R. (2011). Open Babel: an open chemical toolbox. J. Cheminform. *3*, 33. https://doi.org/10.1186/1758-2946-3-33.

O'goshi, K.I., and Serup, J. (2006). Safety of sodium fluorescein for in vivo study of skin. Skin Res. Technol. *12*, 155–161. https://doi.org/10.1111/j.0909-752X.2006.00147.x.

Owen, S.C., Doak, A.K., Wassam, P., Shoichet, M.S., and Shoichet, B.K. (2012). Colloidal aggregation affects the efficacy of anticancer drugs in cell culture. ACS Chem. Biol. *7*, 1429–1435. https://doi.org/10.1021/cb300189b.

Reinhardt, M., Bruce, N.J., Kokh, D.B., and Wade, R.C. (2021). Brownian dynamics simulations of proteins in the presence of surfaces: long-range electrostatics and mean-field hydrodynamics. J. Chem. Theory Comput. *17*, 3510–3524. https://doi.org/10.1021/acs.jctc.0c01312.

Ribeiro, R.P., Coimbra, J.T.S., Ramos, M.J., and Fernandes, P.A. (2017). Diffusion of the small, very polar, drug piracetam through a lipid bilayer: an MD simulation study. Theor.Chem. Acc. *136*, 46. https://doi.org/10.1007/s00214-017-2073-3.

Rojas, M.S., Garcia, R.S., Bini, E., de la Cruz, V.P., Contreras, J.C.L., Pando, R.H., Gonzalez, F.B., Davila-Gonzalez, E., Morales, M.O., Domínguez, A.G.A., et al. (2021). Quinacrine, an antimalarial drug with strong activity inhibiting sars-cov-2 viral replication in vitro. Viruses *13*, 121. https://doi.org/10.3390/v13010121.

Romanowska, J., Kokh, D.B., and Wade, R.C. (2015). When the label matters: adsorption of labeled and unlabeled proteins on charged surfaces. Nano Lett. *15*, 7508–7513. https://doi.org/10.1021/acs.nanolett.5b03168.

Schreier, S., Malheiros, S.V., and de Paula, E. (2000). Surface active drugs: self-association and interaction with membranes and surfactants. Physicochemical and biological aspects. Biochim. Biophys. Acta *1508*, 210–234. https://doi.org/10.1016/S0304-4157(00)00012-5.

Schrödinger Release (2021). QikProp; Schrödinger, LLC: New York.

Seidler, J., McGovern, S.L., Doman, T.N., and Shoichet, B.K. (2003). Identification and prediction of promiscuous aggregating inhibitors among known drugs. J. Med. Chem. *46*, 4477–4486. https://doi.org/10.1021/jm030191r.

Sekula, B., Zielinski, K., and Bujacz, A. (2013). Crystallographic studies of the complexes of bovine and equine serum albumin with 3, 5-diiodosalicylic acid. Int. J. Biol. Macromol. *60*, 316–324. https://doi.org/10.1016/j.ijbiomac.2013.06.004.

Shelley, J.C., Cholleti, A., Frye, L.L., Greenwood, J.R., Timlin, M.R., and Uchimaya, M. (2007). Epik: a software program for pKa prediction and protonation state generation for drug-like molecules. J. Comput. Aided Mol. Des. *21*, 681–691. https://doi.org/10.1007/s10822-007-9133-z.

Soumpasis, D.M. (1983). Theoretical analysis of fluorescence photobleaching recovery experiments. Biophys. J. *41*, 95–97. https://doi.org/10.1016/S0006-3495(83)84410-5.

Sugano, K., Kansy, M., Artursson, P., Avdeef, A., Bendels, S., Di, L., Ecker, G.F., Faller, B., Fischer, H., Gerebtzoff, G., et al. (2010). Coexistence of passive and carrier-mediated processes in drug transport. Nat. Rev. Drug Discov. *9*, 597–614. https://doi.org/10.1038/nrd3187.

Trott, O., and Olson, A.J. (2009). AutoDock Vina: improving the speed and accuracy of docking with a new scoring function, efficient optimization, and multithreading. J. Comput. Chem. *31*, 455–461. https://doi.org/10.1002/jcc.21334.

Unni, S., Huang, Y., Hanson, R.M., Tobias, M., Krishnan, S., Li, W.W., Nielsen, J.E., and Baker, N.A. (2011). Web servers and services for electrostatics calculations with APBS and PDB2PQR. J. Comput. Chem. *32*, 1488–1491. https://doi.org/10.1002/jcc.21720.

van de Weert, M., and Stella, L. (2011). Fluorescence quenching and ligand binding: a critical discussion of a popular methodology. J. Mol. Struct. *998*, 144–150. https://doi.org/10.1016/j.molstruc.2011.05.023.

von Bülow, S., Siggel, M., Linke, M., and Hummer, G. (2019). Dynamic cluster formation determines viscosity and diffusion in dense protein solutions. Proc. Natl. Acad. Sci. USA *116*, 9843–9852. https://doi.org/10.1073/pnas.1817564116.

White, N.S., and Errington, R.J. (2005). Fluorescence techniques for drug delivery research: theory and practice. Adv. Drug Deliv. Rev. *57*, 17–42. https://doi.org/10.1016/j.addr.2004.08.003.

Wilson, K.P., Malcolm, B.A., and Matthews, B.W. (1992). Structural and thermodynamic analysis of compensating mutations within the core of chicken egg white lysozyme. J. Biol. Chem. *267*, 10842–10849. https://doi.org/10.1016/s0021-9258(19)50095-3.

Yadav, S., Shire, S.J., and Kalonia, D.S. (2011). Viscosity analysis of high concentration bovine serum albumin aqueous solutions. Pharm. Res. (N. Y.) *28*, 1973–1983. https://doi.org/10.1007/s11095-011-0424-7.

Zhang, Y., Park, K.Y., Suazo, K.F., and Distefano, M.D. (2018). Recent progress in enzymatic protein labelling techniques and their applications. Chem. Soc. Rev. *47*, 9106–9136. https://doi.org/10.1039/c8cs00537k.

Zhitomirsky, B., and Assaraf, Y.G. (2015). Lysosomal sequestration of hydrophobic weak base chemotherapeutics triggers lysosomal biogenesis and lysosome dependent cancer multidrug resistance. Oncotarget *6*, 1143–1156. https://doi.org/10.18632/oncotarget.2732.

Zimmerman, S.B., and Trach, S.O. (1991). Estimation of macromolecule concentrations and excluded volume effects for the cytoplasm of Escherichia coli. J. Mol. Biol. *222*, 599–620. https://doi.org/10.1016/0022-2836(91)90499-V.

STAR★METHODS

KEY RESOURCES TABLE

REAGENT or RESOURCE	SOURCE	IDENTIFIER
Dulbecco's phosphate-buffered saline (PBS 1X)	Biological Industries	Cat# 02-023-1A
HEPES buffer	Fisher BioReagents	LOT# 170358
DMEM(1X) Gibco	Life Technologies Limited	REF# 41965-039
Fetal Bovine Serum (Gibco)	Life Technologies Limited	REF# 12657-029
Trypsin-EDTA Solution A	Biological Industries	REF# 03-050-1B
Penicillin/ Streptomycin	Biological Industries	REF# 03-031-1B
Sodium Pyruvate Solution	Biological Industries	REF# 03-042-1B
35-mm glass-bottomed dishes	MatTek Corporation	P35G-0-14-C
Pierce™ Dye Removal Columns	Thermo-Fisher scientific	Cat# 22858
Superdex 200 Increase 10\300 GL column	Sigma-Aldrich	GE, Cat# 28-990944
Gebaflex tubes 3.5KDa (GeBa)	TIVAN BIOTECH	Cat# MIDI3-100
Capillary Glass Tubing	Warner Instruments	Model No. G120TF-4 203-776-0664
96- well Black F-Bottom Plate	Greiner-bio-one	REF# 655076
Disposable cuvettes	SARSTEDT AG & Co. KG	REF# 67.742
BSA (Albumin Bovine, fraction V)	MP Biomedicals, LLC	CAS# 9048-46-8
HEWL (Lysozyme from chicken egg white)	Merck	CAS# 12650-88-3
Myoglobin (from equine heart)	Merck	CAS# 100684-32-0
Doxorubicin	AdooQ Bioscience	Cat# A14403
Fluorescein disodium salt	chemcruz	Cat# sc-206026
GSK3 inhibitor SB216763	Abcam	Cat# ab120202
Quinacrine dihydrochloride	Abcam	Cat# ab120749
FluoView	http://www.olympusconfocal.com/applications/index.html	N/A
Kaleidagraph version 4.1 (Synergy).	https://www.synergy.com/features/	N/A
Malvern's Zetasizer software	https://www.malvernstore.com/categories/software	N/A
Simulation of Diffusional Association (SDA) 7 software package version 7.2	https://mcm.h-its.org/sda/	N/A
Schrödinger, LLC, New York, NY	https://www.schrodinger.com/	N/A
Pymol version 1.8.2.3	https://pymol.org/2/	N/A
GAMESS 2017	https://www.msg.chem.iastate.edu/gamess/	N/A
Open Babel 3.0.0	http://openbabel.org/wiki/Main_Page	N/A
AMBER 2016	https://ambermd.org/	N/A
HYDROPRO	http://leonardo.inf.um.es/macromol/programs/hydropro/hydropro.htm	N/A
Pdb2pqr	https://server.poissonboltzmann.org/	N/A
AutoDock Vina	http://vina.scripps.edu/	N/A
Data to run and analyze Brownian dynamics simulations	N/A	ZENODO: 10.5281/zenodo.6953074

RESOURCE AVAILABILITY

Lead contact

Further information and requests for resources should be directed to and will be fulfilled by Gideon Schreiber (gideon.schreiber@weizmann.ac.il). Requests regarding the computational work should be directed to Rebecca Wade (rebecca.wade@h-its.org)

Materials availability

This study did not generate new unique reagents. No plasmids were generated as a part of this study. All other chemical reagents were purchased commercially from the vendors described in the key resources table.

Data and code availability

The code used to perform Brownian dynamics simulations and data analysis of trajectories, Simulation of Diffusional Association (SDA) 7, version 7.2, (Martinez et al., 2015) is available at https://mcm.h-its.org/sda. Input scripts and coordinates have been deposited at: https://zenodo.org/record/6953074#.YukwRmFBw5k

Data reported in this article will be shared by the lead contact on request. Any additional information required to reanalyze the data reported in this article is available from the lead contact on request.

EXPERIMENTAL MODEL AND SUBJECT DETAILS

HeLa cells were used for all in cell FRAP experiments.

METHOD DETAILS

Confocal microscopy and FRAP analysis

Images were collected with an Olympus IX81 FluoView FV1000 Spectral/SIM Scanner confocal laser-scanning microscope, using 60X DIC oil-immersion objective, N.A. 1.35. For fluorescein disodium salt fluorescence measurements, excitation was done at 440 nm using a diode laser at an output power of 1–4% of maximal intensity for high to low concentrations, whereas emission was recorded from 520 to 550 nm using the spectral detection system. For doxorubicin, excitation was done at a 515 nm diode laser using 5–10% of the maximal intensity, and emissions were collected from 540-640 nm. For quinacrine dihydrochloride and GSK3 inhibitor, excitation was done at 488 nm laser using 1–2% of the maximal intensity, whereas emission was collected from 502-560 nm with SDM560 emission dichromator cut off filter. For FRAP measurements while in a drop, the small molecule concentrations used were fluorescein (20 μM), doxorubicin (100 μM), GSK3 inhibitor (20 μM), and quinacrine (30 μM), respectively. Concentration values (depending on the quantum yields of the fluorophores) in the buffer measurements were such that the reading laser (at 515 nm or 440 nm wavelength) should not exceed more than 5% of their full intensities. The protein concentrations were normally varied between 1 mg/mL to 50 mg/mL. Only for BSA, the concentrations varied between (0.01 mg/mL to 200 mg/mL) while with Doxorubicin. All image analyses were performed using FluoView software, and data analyses were performed using Kaleidagraph software version 4.1 (Synergy).

Line-FRAP and classical XY-FRAP

Line-FRAP was carried out in liquid drops. The target drops were imaged applying a 60x differential interference contrast oil-immersion objective lens. For photobleaching, "Tornado" of 4 pixels (2 × 2) diameter was used in the simultaneous stimulus scanner. This is the smallest area achievable using Tornado. The circle area of the bleach was kept precisely in the middle of the scanning line. In most measurements, the unidirectional lines were scanned with time intervals of 1.256 ms 1000 times (equivalent to 1.256 s). The number of scans before, during, and after photobleaching was 10, 42, and 948, respectively. Photobleaching was achieved by the simultaneous laser at 405-nm excitations with 63 millisecond durations, used at full intensity (100%). The simultaneous scanner moved at a speed of 100 μs/pixel to perform an efficient photobleach. We have used two simultaneous scanners during the FRAP experiments: one scanner (at 405 nm with the full intensity of 100%) for photobleaching and another scanner (at 440/515 nm with weak intensity) for data acquisition. For all the drugs, bleach was performed by 405 nm laser, whereas for main excitations, fluorescein 440 nm laser (1–4%); GSK3 inhibitor 440 nm laser (0–1%) were used. Emission collections were done from 520-550 nm for Quinacrine DHC and GSK3 inhibitor. Using the Olympus IX81 FluoView FV1000 Spectral/SIM Scanner confocal laser-scanning microscope with Tornado (which requires SIM scanner to be loaded) greatly enhances bleaching efficiency. In addition, it shortens the time to obtain the first measurement after bleach (which is immediate in this mode). This property is highly beneficial for Line-FRAP measurements, where the time scale of data acquisition plays an important role. The Fluoview SIM scanner unit synchronizes laser light simulation with confocal and multiphoton imaging to avoid interruption to image observation during laser stimulation or manipulation. We have varied the intensity of the lasers to achieve a good signal/noise ratio. Fluorescence recovery plots were fitted to a double exponent growth curve. FRAP

experiments were also performed inside the PBS buffer drops and in crowding conditions. Glass plate dishes containing coverslips are used for microscopic measurements. Calculations of diffusion coefficients from the FRAP rates and averaged bleach sizes are described in calculating diffusion rates and statistical analysis.

Steady-state fluorescence quenching assays

Steady-state fluorescence quenching experiments were carried out on a Tecan fluorescence plate reader instrument. BSA, Myoglobin, and HEWL solutions of 2 μM strength in PBS 1X (pH = 7.4) were prepared. Different small molecules are added in the protein solutions, maintaining the final concentrations between 1 to 100 μM. The final volume of each mixture was strictly 200 μL. The whole set of experiments was performed in a 96-well microplate system (black, flat bottom, Fluotrac). The fluorescence emission spectra were recorded at λ_{exc} = 280 nm and λ_{em} from 300 to 450 nm, with the intensity at 344 nm (tryptophan) being used to calculate the dissociation constant (van deWeert and Stella, 2011). Fluorescence changes upon formation of a 1:1 complex is given by Equation (2)

$$\frac{F_0 - F}{F_0 - F_c} = \frac{[PQ]}{[P]_t} = \frac{[P]_t + [Q]_a + K_d - \sqrt{\left([P]_t + [Q]_a + K_d\right)^2 - 4[P]_t[Q]_a}}{2[P]_t} \quad \text{(Equation 2)}$$

where F is the measured fluorescence, F_0 is the starting fluorescence, F_c is the fluorescence of the fully complexed protein, K_d is the dissociation constant, $[P]_t$ is the concentration of protein, and $[Q]_a$ is the concentration of added ligand/quencher (small molecule/drug in our case). Data were fitted using Kaleidagraph version 4.1 (Synergy). The dissociation constants, K_d, are given in Table S1.

Dynamic light scattering (DLS) measurements

The hydrodynamic size (in nm) of the protein and protein/small molecule complexes in PBS buffer solution was measured using a Malvern's Zetasizer Nano ZSP with a backscatter detection system at an angle of 173°. A minimum of three measurements were recorded for each sample. SARSTEDT disposable cuvettes with 400 μL of the sample were used. The equilibration time was about 15–30 min, and all the measurements were done at 25°C. The hydrodynamic size (in nm) was computed using Malvern's Zetasizer software. Only auto-correlogram profiles (Correlation Function) with good quality fits were taken for final data consideration. Fluorescein:BSA concentration ratios were kept similar to the FRAP experimental conditions. In one measurement, the fluorescein concentration was increased up to 10 times (from 20 μM to 200 μM) that used in FRAP experiments to see if, at a higher concentration, fluorescein can alter the oligomerization state of BSA or not.

Size exclusion chromatography

Proteins (BSA, HEWL, myoglobin each separately), small molecules (fluorescein, doxorubicin, GSK3 inhibitor, quinacrine each separately), and three proteins with all four small molecules in mixtures were loaded onto a Superdex 200 Increase 10\300 GL column (GE, cat 28-990944) by an Alias™ auto-sampler. The highest protein concentration was kept fixed at 5 mg/mL. The small molecule concentrations used were fluorescein (100 μM), doxorubicin (100 & 200 μM), GSK3 inhibitor (80 μM), and quinacrine (80 μM), respectively. The column was pre-equilibrated with PBS 1X (pH 7.4), and the proteins were diluted in the same buffer. UV signals (in mAU, milli-absorbance units) for each size exclusion profile were detected simultaneously at 280 nm and 485 nm wavelengths.

Brownian dynamics simulations

The initial coordinates for HEWL, BSA and myoglobin were obtained from the PDB files 1HEL (Wilson et al., 1992), 4F5S (Bujacz, 2012) and 1DWR (Chu et al., 2000), respectively. Partial atomic charges and protonation states for the protein crowders at pH 7.2 were computed using pdb2pqr (Dolinsky et al., 2004; Unni et al., 2011). Partial atomic charges for the heme group of myoglobin were obtained from previous work (Giammona, 1984).

The initial coordinates for the small molecules were obtained from conversion of SMILES to PDB format using Babel (O'Boyle et al., 2011). The protonation state of the molecules at pH 7.2 was computed using Epik (Shelley et al., 2007) in Maestro (Schrödinger, LLC, New York, 2021). The log P and number of violations to Lipinski's Rule of Five were computed using QikProp in Maestro (Schrödinger, LLC, New York, 2021). The structures of the four small molecules were energy minimized using Maestro and then submitted to

quantum mechanical calculations in GAMESS (Gordon et al., 2005) using HF and the 6-31G** basis set to obtain RESP (Bayly et al., 1993; Cornell et al., 1993) partial atomic charges.

BD simulations were performed using the Simulation of Diffusional Association (SDA) 7 software package (Martinez et al., 2015), version 7.2, available at https://mcm.h-its.org/sda. All simulation boxes had the same composition: 80 small molecules of one type (fluorescein, doxorubicin, quinacrine or GSK3 inhibitor), or 80 small molecules and 440 protein crowders of one type (BSA, HEWL or myoglobin), resulting in a crowder:small molecule ratio of 5.5, which mimics the experimental conditions. Different crowder concentrations were achieved by changing the size of the cubic periodic simulation box (Table S5).

Three replica BD simulations were performed for each system. BD simulations were performed using a time step of 0.5 ps, ionic strength of 190 mM and periodic boundary conditions. Small molecules and proteins were kept rigid, and the same conformations of each small molecule and protein were used for all simulations. The translational and rotational diffusion coefficients of the small molecules and proteins at infinite dilution in aqueous solution, necessary to perform BD simulations, were computed from HYDROPRO (García DeLa Torre, Huertas and Carrasco, 2000), with a radius of the atomic element (AER) of 2.9 Å for proteins and 1.2 Å for small molecules (see details below, Table S6). Hydrodynamic interactions were computed using a mean-field model (Mereghetti and Wade, 2012). The Stokes radii of the small molecules and proteins, necessary to compute hydrodynamic interactions, were calculated from the solvent-accessible volume estimated from a single point Poisson–Boltzmann calculation performed using AMBER 2016 (Case et al., 2016) (Table S2). A radius of four times the Stokes radius of the protein was used to define the local volume for computing hydrodynamic interactions. The forces between molecules were modelled by computing electrostatic interaction, electrostatic desolvation and non-polar desolvation terms from the interactions between the atoms of each molecule and precomputed potential grids on the other molecules. Effective charges computed for the proteins (Gabdoulline and Wade, 1996) and for the small molecules (Ganotra, 2020) were used to calculate electrostatic interactions during the BD simulations. The grid spacing for protein crowders and small molecules was 0.75 Å for simulations with doxorubicin and 0.65 Å for simulations with the other small molecules. The lengths of the sides of the cubic grids for the small molecules were 97 grid points (electrostatic potential) and 80 grid points (for the other, shorter-range potentials). The lengths of the sides of the cubic grids were 161 grid points (electrostatic potential) and 135 grid points (for the other potentials) for HEWL, 225 grid points (electrostatic potential) and 193 grid points (for the other potentials) for BSA, and 225 grid points (electrostatic potential) and 200 grid points (for the other potentials) for myoglobin.

First, all simulated systems were subjected to a 0.2 μs-length BD simulation with interactions between molecules modelled by only a soft-core repulsion energy term to resolve any steric clashes in the initial simulation box generated by the SDA tool genbox. After this, BD production simulations were performed for 10 μs.

The parameters and grids described above were also employed to perform BD simulations in the presence of a silica surface to mimic glass. The parameters for the silica surface were obtained from a previous BD simulation study (Reinhardt et al., 2021), and a similar simulation setup was used here. The silica surface was represented as a homogeneously charged graphite lattice surface with a charge density of -0.0013 e/Å^2. The surface was assigned a charge distribution of -0.0032 e/atom. The x and y dimensions of the simulation box and of the silica surface were 340 Å. The desired crowder concentration was achieved by changing the height (z axis) of the simulation box. In the starting configuration for BD simulations, a buffer region of 120 Å separated the surface and the solutes. Before inclusion of the surface and buffer region in the system, systems were subjected to an initial 0.2 μs-length BD simulation with interactions between molecules modelled by only a soft-core repulsion energy term to resolve any steric clashes in the initial simulation box. After this, BD production simulations were performed for 10 μs. In the analysis of molecule adsorption, a molecule was considered adsorbed when its distance from the surface was less than 4 times the Stokes radius of the molecule (Reinhardt et al., 2021).

For all BD simulations, radial distribution functions and the number of small molecule-protein or small molecule-small molecule contact interactions were computed using SDA7. Contacts were defined as present when heavy atoms (at least one in each molecule) were within a distance of 4.5 Å of each other. Snapshots were analysed at intervals of 500 picoseconds and values averaged over the last 10 microseconds of the simulations.

Computation of diffusion coefficients for small molecules

HydroPro (García De La Torreet al., 2000) was parameterized to reproduce the experimental translational and rotational diffusion coefficients of proteins. One parameter, the radius of the atomic elements (AER), was adjusted to reproduce the experimental results. A procedure similar to that followed in the original publication (García De La Torre et al., 2000) was followed to obtain an AER value for small molecules:

1. Estimate translational diffusion coefficients for small molecules using varying values of AER (1, 2, 3 and 4 Å);
2. Do a linear fit for the graph AER values versus translational diffusion coefficients for each small molecule, and calculate the AER value that reproduces the experimental translational diffusion coefficient;
3. Calculate the final AER value as the average of the AER values obtained for each small molecule. Following the procedure above, an AER value of 1.2 Å was obtained for small molecules. Table S6 shows the computed diffusion coefficients for molecules with known experimental diffusion coefficients (Gray, 1957; Longsworth, 1953) using AER values before and after the reparameterization for small molecules.

Docking of the small molecules to the proteins

Docking was performed using Autodock Vina (Trott and Olson, 2009), a cubic grid with a spacing of 0.375 Å and 70 grid points, and default parameters. The grid was centered on the catalytic site of HEWL (PDB 1HEL) or on one of the four binding cavities of BSA (PDB 4F5S), identified by the presence of 3,5-diiodosalicylic acid in the complex with BSA in PDB 4JK4 (Sekula et al., 2013). The docking pose with the highest score was retained.

QUANTIFICATION AND STATISTICAL ANALYSIS

Calculating diffusion rates and statistical analysis

The apparent diffusion coefficients derived from FRAP measurements are $D_{confocal}$ (Dey et al., 2021), which are calculated according to Equation 1 (see introduction). The bi-exponential function was used to fit the data. The two rate constant parameters, k_1 and k_2, with their associated amplitudes (a_1 and a_2) were used to calculate $\tau_{1/2}$ using Equation 3.

$$\frac{1}{\tau_{1/2}} = \frac{p1}{\tau(1)_{1/2}} + \frac{p2}{\tau(2)_{1/2}} \quad \text{(Equation 3)}$$

where p_1 and p_2 are the fraction amplitudes of k_1 and k_2, and $\tau(1)_{1/2}$ and $\tau(2)_{1/2}$ are the respective half-recovery times. The bleach sizes are calculated from the Equation (4). To improve the signal to noise, we averaged 30 independent measurements and fitted them to a Gaussian (Equation 4):

$$f_x = A^0 + Ae^{-\frac{(x-b)^2}{2c^2}} \quad \text{(Equation 4)}$$

where A^0 is the offset, A the amplitude, b the midpoint and c the width, which is related to the width at half maximum (FWHM) by FWHM = $2(2\ln 2)^{1/2}c$. This resulted in good Gaussian fits for post-bleach fluorescence profiles for 10, and 63 ms of bleach pulses. Using the fitted c parameter in Equation 4, we found that r_n and r_e should be assigned considering the width at 60% of the post-bleach Gaussian distribution profile, which is equal to 1.38*c. Accordingly, the r_n values for 10, and 63 ms bleach pulses calculated from the Gaussian fits are 0.745, and 1.27 μm (Dey et al., 2021). Similarly the r_e values are calculated using the same equation like previous work (Dey et al., 2021). To calculate $D_{confocal}$ at least 30 independent measurements on different cells (n) were binned, and the curve fit of the progression curve was used to obtain $\tau_{1/2,}$ and r_e values and their associated errors. r_n was obtained from bleaching a fixed sample. The standard errors (SE) of the individual parameters were combined to obtain $D_{confocal} \pm$SE. To verify SE values, we repeated the 30 measurements independently multiple times, which gave the same SE as obtained from individual curve fits of n = 30 cells.